Journal of Modern Science

Tamil Nadu State Council for Higher Education

Chennai - 600 005

JOURNAL OF MODERN SCIENCE

ARTICLES

GUIDELINES FOR SUBMISSION OF MANUSCRIPTS

1. Manuscripts should be submitted in duplicate. It must be typed on one side only, double-spaced, with sufficient margins on all sides to facilitate editing and styling.

2. Charts, tables, etc., and photographs should be numbered consecutively in Arabic numerals. A short title should be provided at the bottom of each page. Photographs must be of good quality. Original charts, tables, etc., will be required for printing.

3. Foot notes or End notes may be used. But it is advisable to use parenthetical documentation as recommended by Science Citation Index (SCI) for Research papers. Notes should be worked into the text if they help clarity. References or works cited should be given at the end of the text and consolidated into a final alphabetized section.

4. All articles are, as a rule, referred to experts for peer review in the subjects concerned. Those recommended by the referees alone will be published in the Journal after appropriate editing.

5. A declaration stating that the article has not been submitted elsewhere should accompany the manuscript.

6. Submission of an article does not guarantee publication.

HYDROTHERMAL SYNTHESIS OF CdO@ZnO CORE-SHELL PARTICLES AND THEIR PHOTOCATALYTIC AND BACTERICIDAL ACTIVITIES

A.Vijayabalan

Abstract

The CdO@ZnO core-shell is prepared by hydrothermal method and characterized by XRD, HR-SEM, DRS, PL and Impedance spectra. The deep level emission (DLE) is more for CdO@ZnO core-shell than ZnO. The core-shell shows larger bactericidal activity than pristine ZnO and CdO.

Keywords

UV-A light, CdO, ZnO, Rhodamine-B, E.coli

1. Introduction

CdO is an n-type semiconductor with a direct band gap of 2.5 eV and an indirect band gap of 2.0 eV [1]. CdO nanostructures have low ohmic resistivity and high optical transmittance. With a moderate refractive index it offers excellent properties for applications in optoelectric devices like transparent electrodes, photovoltaic cells, phototransistors and photodiodes. The small band gap enables CdO to get photoexcited under visible light and act as photocatalyst. Phenols [2-4], naphthol [5] and organic dyes such as pyronine B and safranine T [6] are photodegraded by CdO. The visible light-photocatalytic activities and the bactericidal activities of the composites are larger than their precursors. CdS/TiO$_2$ heterostructures shows a superior hydrogen evolution rate from water splitting to single CdS or TiO$_2$ due to the efficient electron transfer from CdS conduction band (CB) to TiO$_2$ CB and the wide light absorption of CdS itself [7]. Recently, wedemonstrated that a ZnO–CdS heterostructure photocatalyst based on direct Z-scheme mechanism exhibits wide light response and high hydrogen evolution by prolonging lifetime of charge carriers.

* *St.Joseph's College of Arts and Science (Autonomous) Manjakuppam, Cuddalore, Tamilnadu-607001*

For heterostructured photocatalysts, besides the mechanisms of charge carrier transfer, two more aspects can also play key roles in determining overall hydrogen evolution rate from photocatalytic water splitting, in particular for long-term applications. One is the stability of semiconductor units in heterostructures upon light irradiation. It is well known that both CdS prepared by traditional routes and ZnO as photocatalysts usually suffer from serious photocorrosion in longterm photocatalytic reactions [8]. The instability problem caused by photocorrosion also exists in our previously developed ZnO–CdS heterostructure photocatalysts [9]. However, the stability of CdS can be changed depending on preparation routes. For example, Jing et al. reported that CdS with steps on particle surface, prepared by a solid state reaction route, shows an ultra-high stability and activity in hydrogen evolution from water splitting [10]. Therefore, it is expected that the stability of ZnO–CdS heterostructures can be probably improved by employing different preparation routes. ZnO–CdS core–shell hybrid nanorods as an efficient photocatalyst for hydrogen evolution from water splitting. In contrast to the previously developed ZnO–CdS heterostructures containing only ZnO/CdS nanoparticles prepared by wet chemistry route [9], ZnO–CdS core–shell nanorods show very stable hydrogen evolution in a long-term reaction under the irradiation of simulated solar light.

2. Materials and methods

2.1. Materials

Zinc nitrate (Hi-media), Cadmium nitrate (Sd-fine), hexamine (Hi-media), Cetyltrimethylammonium bromide (Hi-media), liquid ammonia (Qualigens), oxalic acid (Merck) were used. Commercially available ethanol was distilled over CaO. MacConkey agar (Hi-media) and nutrient broth (SRL) were used as supplied. Doubly distilled deionized water was employed throughout the experiments. Other chemicals used were also of analytical or reagent grade.

2.2 .Methods

Preparation of CdO@ZnO core-shell by hydrothermal method

To CdO nanoparticles suspended in distilled ethanol (0.1 g in 10 mL) under sonication for 10 min, aqueous solution of $Zn(NO_3)_2$ (5 g in 15 mL) was added drop wise with stirring. Then aqueous oxalic acid (0.5 M, 50 mL) solution was added to precipitates zinc oxalate. This was followed by cetyltrimethylammonium bromide (CTAB) in ethanol (10 mL, 0.01 M), also under stirring for 1 h. The contents were transferred to a Teflon lined stainless steel autoclave vessel (100 mL) and heated at 150 °C for 14 h in an air oven. After allowing to cool at room temperature,

the crystals were collected by filtration, washed, dried and calcined at 500 °C for 2 h in a muffle furnace fitted with a PID temperature controller.

3. Result and discussion

3.1. Structural analysis

The X-ray diffraction pattern of CdO@ZnO core-shell particles shown in the fig.1. It shows the crystal structure of the ZnO shell as primitive hexagonal crystal lattice with cell parameters *a* and *b* as 0.3249 nm and *c* as 0.5205 nm. The XRD pattern matches totally with the standard JCPDS pattern of zincite (89-7102). The X-ray diffractogram of CdO@ZnO core-shell particles, prepared by hydrothermal method (HT) using cetyltrimethylammonium bromide (CTAB) as templating agent, is shown in fig.1(c). The peaks match with those of zincite (JCPDS no. 89-7102) revealing the shell as ZnO wurtzite shown in fig.1 (b). The X-ray diffractogram of the CdO precursor used to synthesis the core-shell particles, is displayed in Fig.1 (a). The displayed XRD matches with face centered cubic lattice of CdO (JCPDS no. 65-2908), confirming the crystal structure of core CdO. The diffractograms show the ZnO, as zincite ZnO. The diffraction peaks match with those of JCPDS card no. 89-7102 revealing the primitive hexagonal crystal structure with lattice parameters *a* and *b* as 0.3249 nm and *c* as 0.5205 nm. The mean crystallite sizes of the hydrothermally synthesized CdO@ZnO,ZnO and CdO have been deduced from the half-width of the full maximum of the most intense peaks of the respective crystals using the scherrer equation, $D = 0.9\lambda / \beta \cos \theta$. Where, D is the mean crystallite size, λ is the wavelength of X-ray, θ is the bragg angle and β is the corrected half peak width of the experimental sample. The average crystal sizes of ZnO and CdO are 58 and 57 nm respectively.

3.2. Microstructure

The high resolution scanning electron microscopic (HR-SEM) images of CdO@ZnO core-shell particles, at different magnifications shown in the fig.2 The core-shell particles are mostly of submicron size in fig 2(a). Some display hexagonal plate like structure in fig 2(b) but most of them are of irregular shape in fig 2(c). A few nanoparticles are also seen in some HR-SEM images. This suggests that the nanoparticles formed fuse together under hydrothermal condition to yield submicron particles.

The energy dispersive X-ray (EDX) spectra of CdO@ZnO nanoparticles are shown in Fig.3. It is confirms the presence of ZnO shell in the prepared core-shell particles. They display the presence of Zn and the absence of Cd. The unlabelled peak corresponding to binding energy of 2.2 keV is that of sputtered gold nanoparticles. The core CdO is deeply buried underneath the ZnO
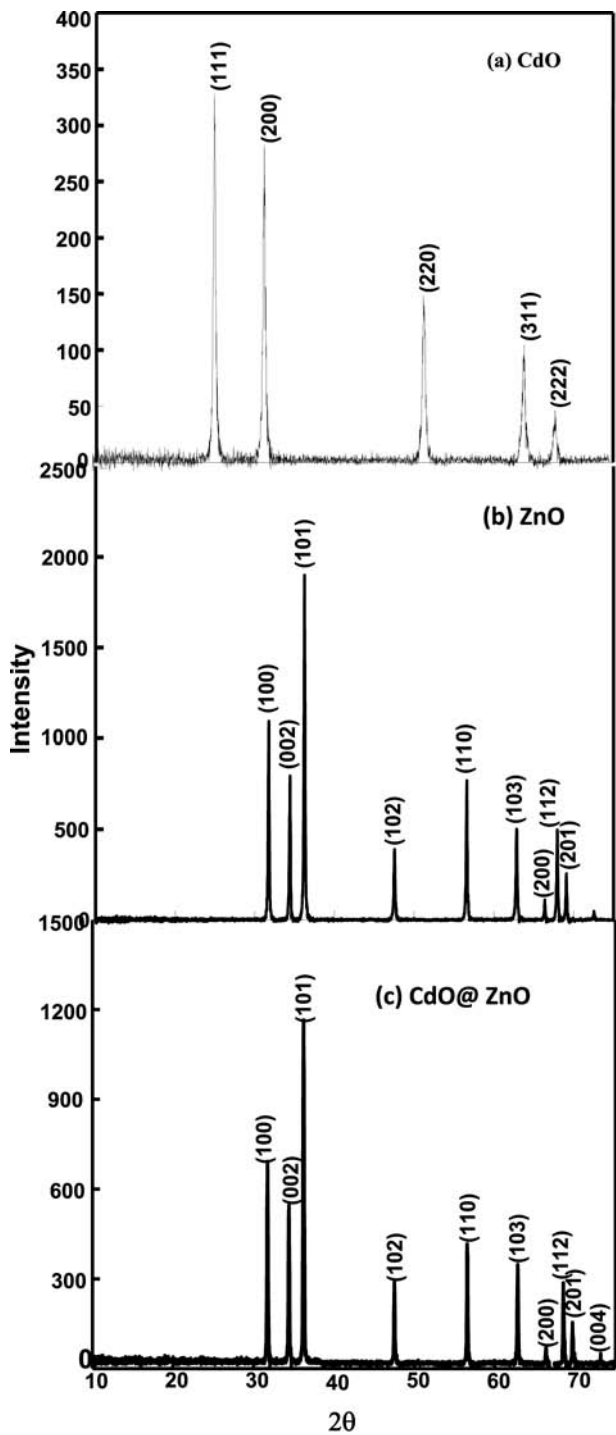
Fig. 1. XRD spectra
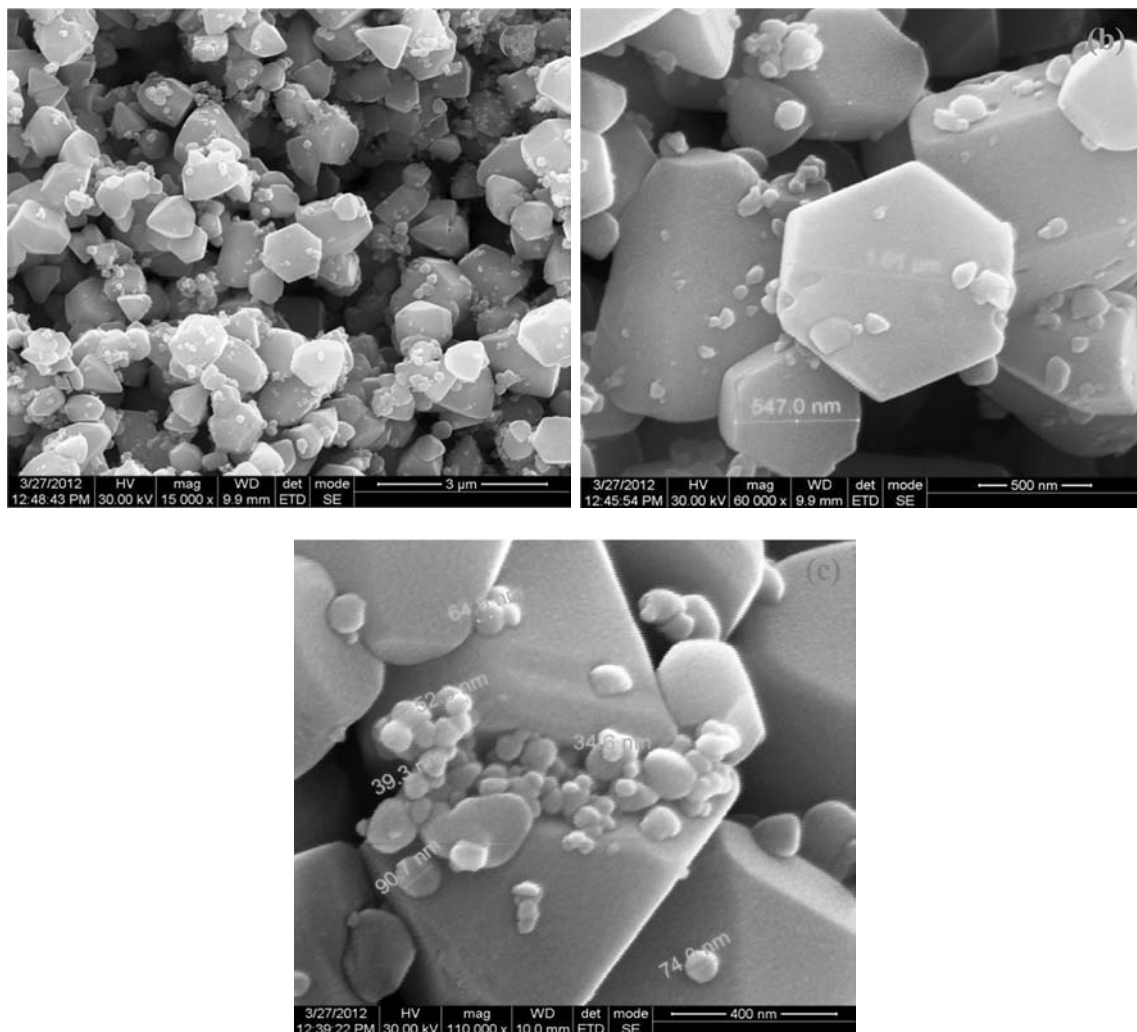
Fig. 2. HR-SEM images of hydrothermally synthesized CdO@ZnO

shell and the X-rays employed in the EDX analysis do not penetrate beyond the ZnO shell. It is known that X-rays penetrate only a few interplanner distances in crystals, which correspond to a few nanometers of the ZnO shell.

3.3. Band gap

The diffuse reflectance spectra (DRS) of CdO@ZnO core-shell particles are shown in Fig.4. The DRS are presented in terms of $F(R)$, obtained by the application of Kubelka-Munk algorithm $F(R) = (1 - R^2)/2R$, where R is the reflectance. The DRS of core-shell particles show that they absorb UV-A light but not visible light. This confirms the ZnO shell in the prepared core-shell
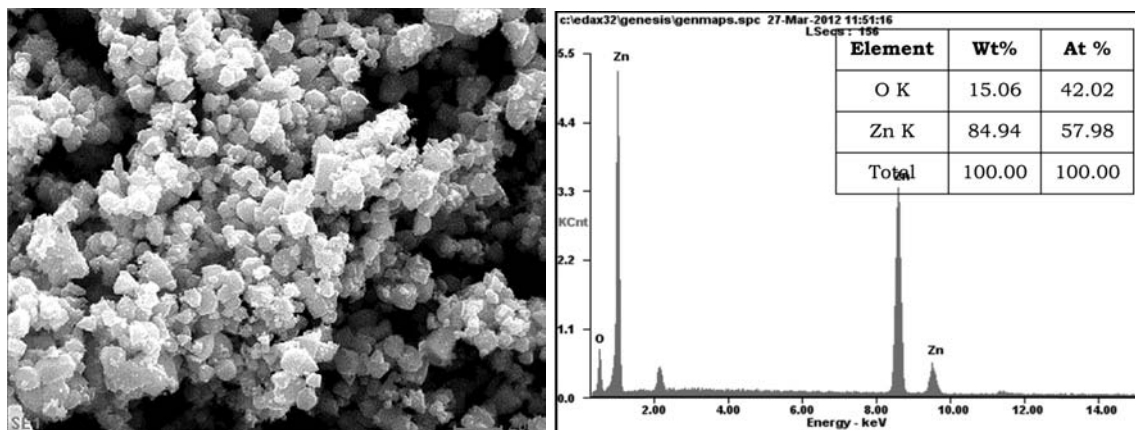
Fig.3. The EDX spectra of CdO@ZnO core-shell

particles. Also, it infers that the synthesized materials are not CdO-ZnO composites; CdO absorbs visible light. The direct band gaps of CdO@ZnO particles, have been deduced from Tauc plots of $[F(R)h\acute{\imath}]^2$ *versus h\'{\i}*, as displayed in Fig.5.The Tauc plots of $[F(R)h\acute{\imath}]^{0.5}$ *versus* photon energy, which give the indirect band gaps of the core-shell oxides shown in Fig.6. The deduced band gaps of CdO@ZnO are comparable with that of ZnO but not with that of precursor CdO. This confirms the perfect ZnO shell of the synthesized core-shell particles. The direct and indirect band gaps of CdO are deduced through Tauc plots as shown in Figs. 5 and 6. respectively.
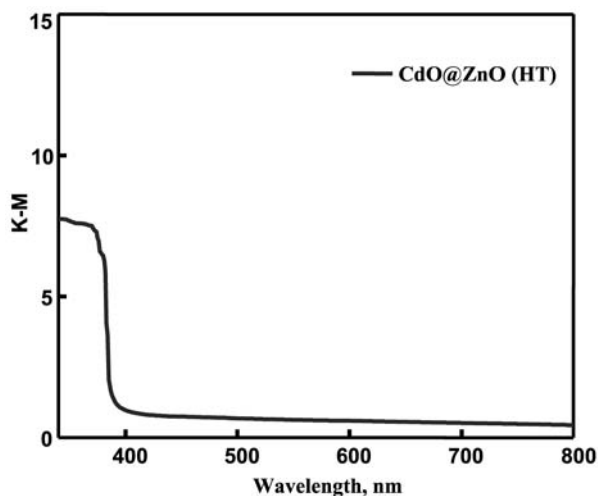
Fig.4. Diffuse reflectance spectra of CdO@ZnO core-shell
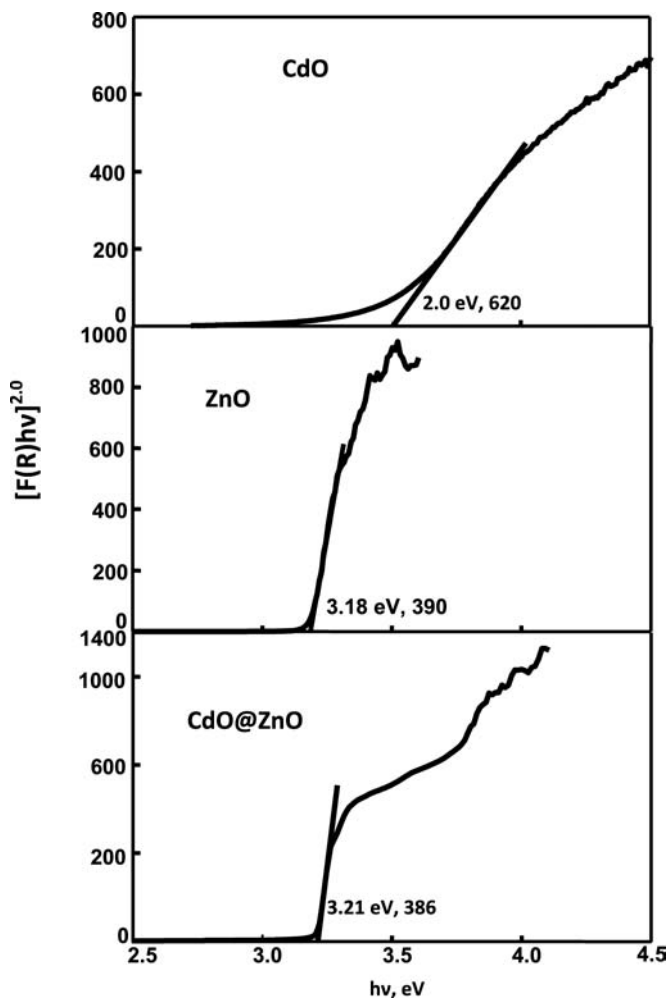
Fig.5. Tauc plot for direct band gap of CdO@ZnO

3.4. Photoluminescence

The photoluminescence (PL) spectra of CdO@ZnO core-shell particles are presented in Fig.7. shows the PL spectra of ZnO adopting the procedure followed for the synthesis of core-shell oxides but without using CdO. The emission spectrum of CdO@ZnO is similar to that of bare ZnO. The CdO@ZnO and ZnO show near band gap emission (NBE) at 420 nm. This is due to excitonic recombination [11].These emissions are close to the band gap absorptions, shown by the Kubelka-Munk plots. Further, they show blue or deep level emission (DLE) at range between 482-484 nm. The visible emission is due to the recombination of electron in singly occupied
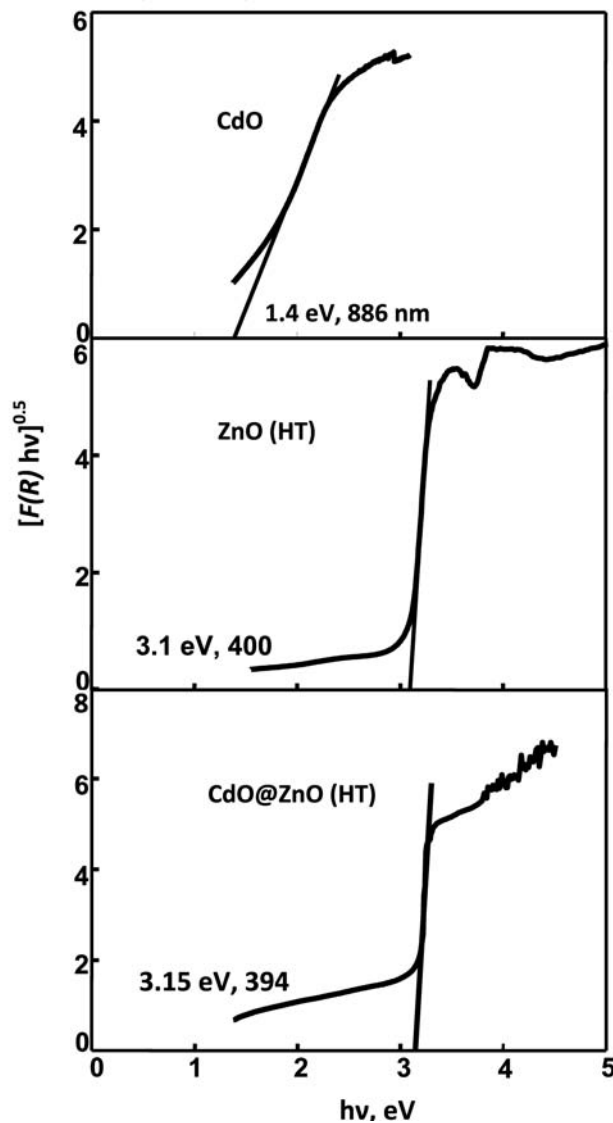
Fig.6. Tauc plot for indirect band gap of CdO@ZnO core-shell

oxygen vacancy with the photogenerated hole in the VB. The DLE is strong for CdO@ZnO than pristine ZnO. The DLE is related to structural defects and strong DLE indicates more defects [12]. The pristine ZnO is likely to be more crystalline and less defective than ZnO in hydrothermally synthesized CdO@ZnO.
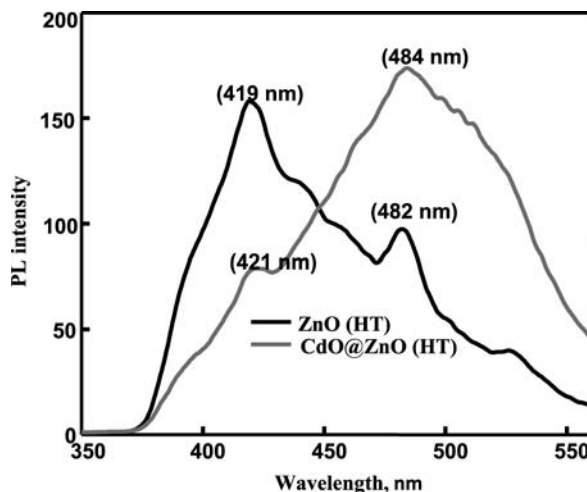
Fig.7. Photoluminesence spectra of CdO@ZnO core-shell

3.5. Photocatalytic activity

The photocatalytic activities of CdO@ZnO particles have been examined under UV-A light using rhodamine B as test substrate are shown in the Fig.8. The results are corrected for adsorption. The profiles of dye degradation on pristine ZnO and CdO precursor are also presented in Figs.8. for comparison. The photocatalytic activity of CdO@ZnO is less than ZnO. As expected CdO, shows poor photocatalytic activity. Generally CdO is a less efficient photocatalyst [13]. Photoformation of electron-hole pairs, their recombination, interfacial charge transfer, light absorption efficiency, adsorption of water molecule, molecular oxygen and dye molecule, etc., determines the photocatalytic efficiency of a semiconductor. ZnO is a better photocatalyst than CdO. The conduction band (CB) electron in ZnO is more cathodic than that of CdO and also the valence band (VB) hole of ZnO is more anodic than that of CdO. This is expected to decrease the photocatalytic activity. That is, the core-shell oxides are to be less photocatalytically active than pristine ZnO. The photoexcited electron in the CB of ZnO in CdO@ZnO is expected to move to the CB of CdO. Similarly, the photogenerated hole in the VB of ZnO in CdO@ZnO is expected to slip to the VB of CdO [14].The energy positions of the CB edges and VB edges of ZnO and CdO on the absolute vacuum scale (AVS) is presented in Fig.9. They determine the charge transfer from ZnO to CdO. The energy difference between the CB electrons of ZnO and CdO is the driving force for the interparticle electron injection and the free energy change is given by $\Delta G = e[E_{CB(CdO)} - E_{CB(ZnO)}]$[14]. Similarly, the energy difference between the VB holes of ZnO and CdO is responsible for the interparticle hole injection. This movement of photogenerated electron and hole from ZnO
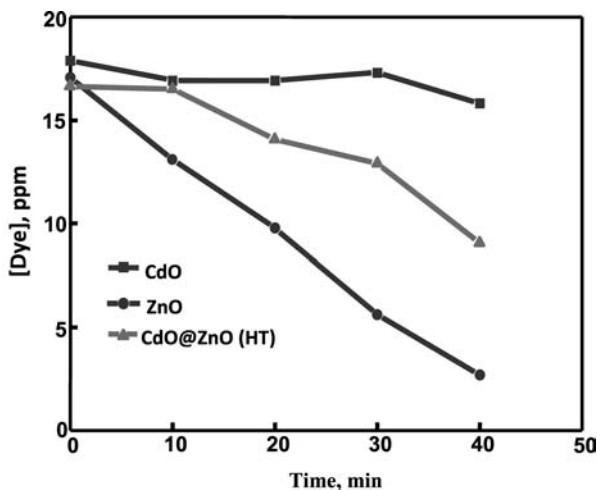
Fig. 8. Temporal profiles of degradation of rhodamine B on hydrothermally synthesized CdO@ZnO

Oxide loading = 0.020 g, $[O_2]_{dissolved}$ = 9.3 mg L^{-1}, airflow rate = 7.8 mL s^{-1},

λ = 365 nm, I = 25.4 ìeinstein L^{-1} s^{-1}, pH = 5.5, volume of dye solution = 25 mL.
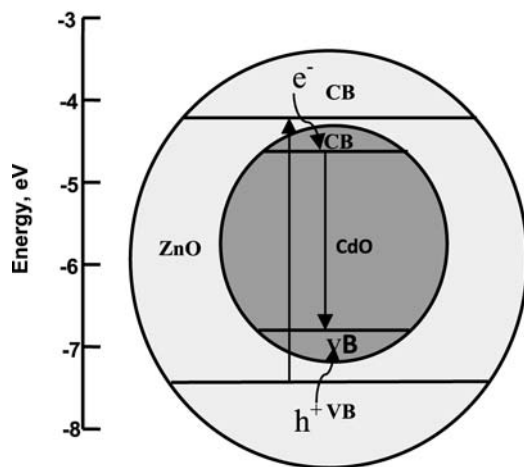
Fig.9. Absolute Vacuum Scale (AVS) of CdO@ZnO core-shell

shell to CdO core should result in recombination of the photogenerated charge carriers in CdO core thus suppressing the photocatalytic activity. This is observed in hydrothermally synthesized CdO@ZnO.

3.6. Bactericidal activity

The time profiles of *E. coli* disinfection by CdO@ZnO shown in the figs.10. The displayed disinfections are by the core-shell particles in aqueous suspension in absence of direct illumination. The corresponding profile of *E. coli* inactivation by pristine ZnO and CdO are also shown in Figs. for comparison. In absence of the particles the *E. coli* population remains unaffected during the experimental period displaying the bactericidal activity of the particles tested. *E. coli* bacteria in 0.9% saline were used for the evaluation of the bactericidal activity. The cell population was determined by a viable count method on MacConkey agar plates after proper dilution of the culture. The temporal profiles show larger bactericidal activity of CdO@ZnO than pristine CdO and ZnO.
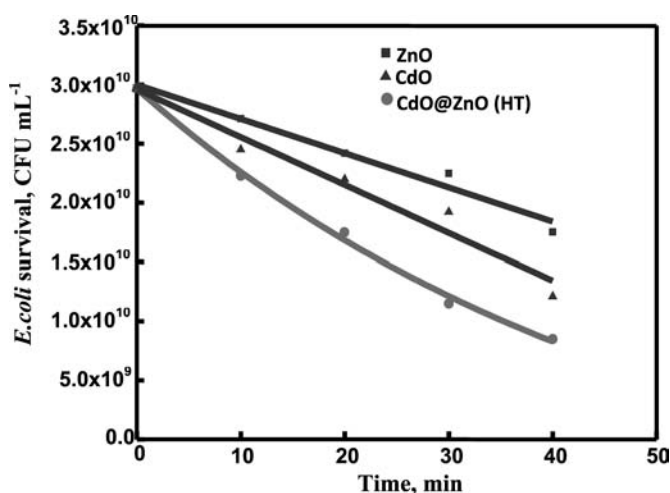
Fig. 10. Temporal profile of *E. coli inactivation* by hydrothermally Synthesized CdO@ZnO under dark

Oxide loading = 0.020 g, pH = 7.1, volume of *E.coli* solution = 25 mL

4. Conclusion

The prepared CdO@ZnO core-shell was confirmed by XRD and EDX. The photocatalytic degradation of rhodamine B was suppressed and *E.coli* was enhanced by core-shell in UV and dark respectively. The deep level emission is strong for CdO@ZnO core-shell.

Reference

1. M.E. de A. Reyes, G.T. Delgado, R.C. Perez, J.M. Marin, O.Z. Angel, Optimization of the photocatalytic activity of CdO + CdTiO$_3$ coupled oxide thin films obtained by sol-gel technique, J. Photochem. Photobiol. A 228 (2012) 22-27.

2. C. Karunakaran, R. Dhanalakshmi, Semiconductor-catalyzed degradation of phenol with sunlight, Solar Energy Mater. Solar Cells 92 (2008) 1315-1321.

3. C. Karunakaran, R. Dhanalakshmi, Selectivity in photocatalysis by particulate semiconductors, Cent. Eur. J. Chem. 7 (2009) 134-137.

4. C. Karunakaran, R. Dhanalakshmi, P. Gomathisankar, G. Manikandan, Enhanced phenol-photodegradation by particulate semiconductor mixtures: Interparticle electron-jump, J. Hazard. Mater. 176 (2010) 799-806.

5. C. Karunakaran, S. Narayanan, P. Gomathisankar, Photocatalytic degradation of 1-naphthol by oxide ceramics with added bacterial disinfection, J. Hazard. Mater. 181 (2010) 708-715.

6. J. Li, Y. Ni, J. Liu, J. Hong, Preparation, conversion, and comparison of the photocatalytic property of $Cd(OH)_2$, CdO, CdS and CdSe, J. Phys. Chem. Solid. 70 (2009) 1285-1289.

7. Gillot. B, Thiebaut. D, Laarj. M, Synthesis of stoichiometric cadmium substituted magnetites and formation by oxidation of solid solutions of cadmium ferrite and ã iron oxide, Thermochim. Acta 342 (1999) 167-174.

8. Reber JF, Meier K. Photochemical hydrogen-production with platinized suspensions of cadmium-sulfide and cadmium zinc-sulfide modified by silver sulfide. J Phys Chem 1986;90(5):824–34.

9. Wang XW, Liu G, Chen ZG, Li F, Wang LZ, Lu GQ, et al.Enhanced photocatalytic hydrogen evolution by prolonging the lifetime of carriers in ZnO/CdS heterostructures. Chem Commun 2009;(23): 3452–4.

10. Jing DW, Guo LJ. A novel method for the preparation of a highly stable and active CdS photocatalyst with a special surface nanostructure. J Phys Chem B 2006;110(23):11139–45.

11. Sun. T, Qiu. J and Liang. C,Controllable fabrication and photocatalytic activity ZnO nanobelt arrays, *J.Phys.Chem.C,* **2008**,*112*,715.

12. M-K.Lee, T.G.Kim,W.Kim and Y-M,Sung, Doping effect of Ag^+,Mn^{2+} ions on structural and optical properties of ZnO nanoparticles, *J.Phys.Chem.C*,**2008,***112,*10079

13. C.Karunakaran, S.Senthilvelan,S.Karuthapandian and K.Balaraman, Solar radiation catalysed aereobic photooxidation of 1-napthol on some semiconductor,*Catal.Commun.***2004**, *5*,283.

14. R.Katosh, A.Furube, T.Yoshihara, K.Hara, G.Fujihashi, S.Takano, S.Murata, H.Arakawa and M.Tachiya, *J.Phys.Chem.B*; **2004,** *108*, 4818.

WIRELESS CONTROLLED SURVEILLANCE ROBOT WITH VIDEO INTERFACE USING ZIGBEE

[1]**C. Rajalakshmi** [2]**Dr.M.Germanus Alex**

Abstract

This thesis implements concept of rolling type robot with multi-motors. The movement of the robot is controlled by four DC motors. The robot uses Zigbee module for wireless transmission whose transmitter is a PC/laptop. Robot can be used for spying in industrial sectors, for research in deep caves and for surveillance in military war fields. This module also contains video reception technique for receiving the live video from the camera attached to the robot. Video signals can be received by an AV receiver and can be viewed at the PC. The range of surveillance is nearly 30-40meters. The distance can be adjusted and varied by strength of the signal. It carries a wireless 360 degree rotatable camera to send a live footage back to the controller. Robot uses Zigbee protocol for sending and receiving signals. Zigbee is an 802.11.4 standard wireless communication, provides low power usage. Mesh networking provides high reliability and more extensive range.

Keywords

Zigbee , Embedded systems, Networks, Microprocessor

1. INTRODUCTION

1.1 Introduction

The main aim of this paper is to control the robot with PC through Hyper Terminal using **Zigbee** wireless technology. Robot can move either forward or backward, Left or right through the set of commands given from the PC through the Hyper Terminal.

The advent of new high-speed technology and the growing computer Capacity provided realistic opportunity for new robot controls and realization of new methods of control theory.

[1] *Prof Department of computer science, Kamarajar Government Arts College, Surandai.*

[2]*Prof & Head of the Department of Computer science, Kamarajar Government Arts College, Surandai. Corresponding Author : rajiamdr@gmail.com*

This technical improvement together with the need for high performance robots created faster, more accurate and more intelligent robots using new robots control devices, new drives and advanced control algorithms. This project describes a new economical solution of robot control systems. The presented robot control system can be used for different sophisticated robot applications.

The control system consists of a PC, a microcontroller that collects data from the PC and wirelessly controls the robot. A complete solution of a robot control solution is presented in this project. The robot was fully controlled by the PC and the commands from the PC were received by the microcontroller through **Zigbee** transceiver.[3]

1.2 Embedded system

An embedded system is a computer design to perform one or a few dedicate functions often with real-time computing constraints. It is embedded as part of a complete device often including hardware and mechanical parts. By contrast, a general purpose computer, such as a personal computer (PC), is designed to be flexible and to meet wide range of end-user needs. Embedded system control many device in common use today.

Embedded systems are controlled by one or more main processing cores that are typically either microcontrollers or digital signal processors (DSP). The key characteristic, however, is being dedicated to handle a particular task, which may require very powerful processors. For example, air traffic control systems may usefully be viewed as embedded, even though they involve mainframe computers and dedicated regional and national networks between airports and radar sites.

1.3 Applications of Embedded Systems

Consumer applications

At home we use a number of embedded systems which include microwave oven, remote control, VCD players, DVD players, Camera etc.,

Office automation

We use systems like facsimile, modem, printer etc.,

Industrial automation

Today a lot of industries are using embedded systems for process control. In industries we design the embedded systems to perform a specific operation like monitoring temperature, pressure,

humidity, voltage, current etc., and basing on these monitored levels we do control other devices, we can send information to a centralized monitoring station. In critical industries where human presence is avoided there we can use robots which are programmed to do a specific operation.[2]

Computer Networking

Embedded systems are used as bridges, routers etc.,

Telecommunications

Figure 1.2 : Telecommunications

A communications network is a collection of transmitters, receivers, and communications channels that send messages to one another. Some digital communications networks contain one or more routers that work together to transmit information to the correct user. An analog communications network consists of one or more switches that establish a connection between two or more users. Cell phones, web cameras etc.,

2. CONCEPTUAL ANALYSIS

2.1 System analysis

Existing System

When we consider the existing system of surveyor robot it consists of a simple camera fixed which is not rotatable

i. Here the video transmission and control of the robot are in separate module, hence the operation increases

ii. A power supply system with a battery to supply power

iii. The traditional surveyor had some disadvantages in power consumption that it becomes inactive when the battery is down

iv. Another thing is that it was unable to make a record of the captured video and automatically change its position according to the obstacle in the front[1]

Proposed System

   i.   The robot we propose consists of a solar charging system with a rechargeable battery for uninterrupted surveillance

   ii.   We use the zigbee module to transmit the controls to the robot

   iii.   A 360 degree rotatable camera is used for complete surveillance in all directions

   iv.   The video transmission and the control system for the robot are done both by a computer interface

   v.   We have a temperature and humidity sensor to sense the situation and give a pre information to the operator

2.2 Motivation

The motivations are either automated or controlled droids that can be used for recon or remote attacks in heavy war zones or spying.

The advantage of using an Unmanned Surveillance Vehicle, relative to use of a manned security system are:

   i.   Does not need a human spy or researcher to risk his/her life

   ii.   Can enter environments that are dangerous to human life

   iii.   Reduces the exposure risk of the experimenter

   iv.   Can perform a precise, repetitive raster scan of a region, day-after-day, night-after-night in complete fog, at high temperature and humidity under computer control:

       1) Performing a geological survey

       2) Performing visual imaging of a region

       3) Measuring the temperature and gas over any terrain

   v.   Can be programmed to complete the mission autonomously even when contact with its CGS is lost

2.3   Robotics

The word "beam" in **BEAM robotics** is an acronym for **B**iology, **E**lectronics, **A**esthetics, and **M**echanics. This is a term that refers to a style of robotics that primarily uses simple analogue circuits, such as comparators, instead of a microprocessor in to produce an unusually simple design (in comparison to traditional mobile robots) that trades flexibility for robustness and efficiency in

performing the task for which it was designed. Exceptions to the convention of using only analog electronics do exist and these are often colloquially referred to as "mutants". BEAM robots typically consist of a set of the aforementioned analog circuits (mimicking biological neurons) which facilitate the robot's response to its working environment.

3. HARDWARE DESCRIPTION

3.1 PC controlled wireless Robot

PC controlled wireless Robot

1. Transmitter section
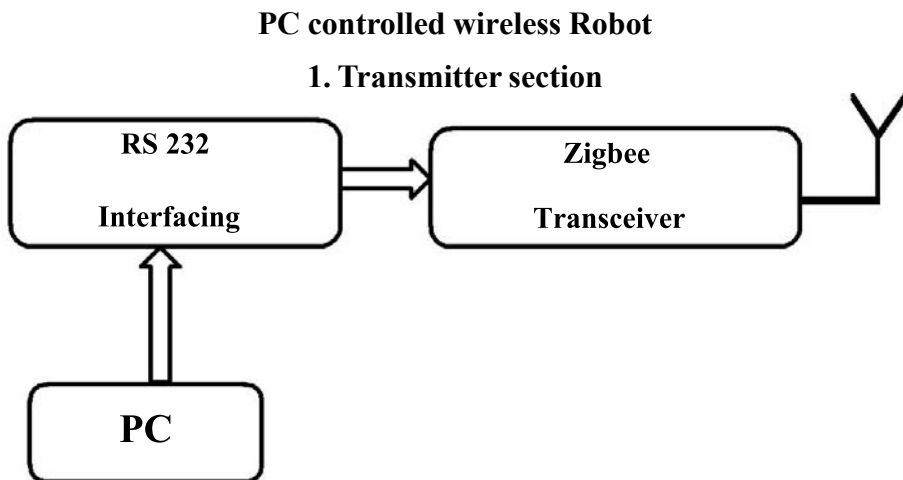
Figure 3.1.1: Block diagram of transmitter section of controlled wireless robot

In this paper the block diagram of the project and design aspect of Independent modules are considered. Block diagram is shown in fig: 2.1:

3.2 The main blocks of this paper are

1. Micro controller (16F877A)

2. Reset button

3. Crystal oscillator

4. Regulated power supply (RPS)

5. Led indicator

6. DC Motors and DC motor drivers

7. RS 232 cable

8. RF transceiver module

3.3 Microcontroller
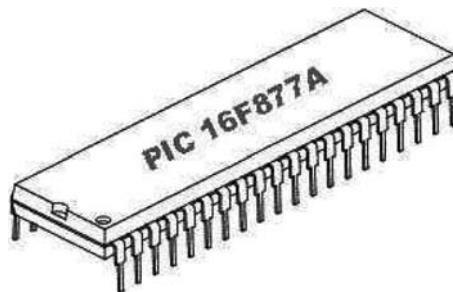
Figure 3.3.1: 16F877A Microcontroller

Circumstance that we find ourselves in today in the field of microcontrollers had their beginnings in the development of technology of integrated circuits. This development has made it possible to store hundreds of thousands of transistor into one chip. That was a prerequisite for production of microprocessor, and the first computer were made by adding external peripherals such as memory, input-output lines, and timers and other. Further increasing of the volume of the package resulted in creation of integrated circuits. These integrated circuits contained both processor and peripherals. That is how the first chip containing a microcomputer, or what would later be known as a microcontroller came about.

Microprocessors and microcontrollers are widely used in embedded systems product. Microcontroller is a programming device. A microcontroller has a CPU in addition to a fixed amount of RAM, ROM, I/O Ports and a timer embedded all on a single chip. The fixed amount of on-chip ROM, RAM and number of I/O Ports in microcontrollers makes them ideal for many applications in which cost and space are critical. The microcontroller used in this project is PIC 16F877A. The PIC families of microcontrollers are developed by Microchip Technology Inc. Currently they are some of the most popular microcontrollers, selling over 120 million devices each year. There are basically four families of PIC microcontrollers:

PIC12CXXX 12/14 –bit program word

PIC16C5XX 12 –bit program word

PIC16CXXX and PIC16FXXX 14 –bit program word

PIC17CXXX and PIC18CXXX 16 –bit program word

The features, pin description of the microcontroller used are discussed in the following sections.[2]

3.4 General Purpose Microprocessor

1. CPU for computers

2. No RAM, ROM, I/O on CPU chip itself

   Example: Intel'sx0   x86,   Motorola's

PIC16F belongs to a class of 8-bit microcontrollers of RISC architecture.It's general structure is shown on th It's used for storing a written pro technology can be programmed and cleared more than once, it makes this microcontroller suitable for device developer.

EEPROM –data memory that needs to be saved when there is no supply. It is usually used for storing important data that must not be lost if power supply suddenly stops. For instance, one such data is an assigned temperature in temperature regulators. If during the loss of power supply this data was lost, we would have to make the adjustment once again upon return of supply. Thus our device loose on self-reliance.[4]

RAM – Data memory used by a program during its execution. In RAM are stored all inter-results or temporary data during run-time.

PORT A and PORT B are physical connections between the microcontroller and the outside world. PORT A has five, and PORT B has eight pins.

FREE-RUN TIMER is an 8-bit register inside a microcontroller that works independently of the program. On every fourth clock of the oscillator it increments its value until it reaches the maximum (255), and then its starts counting over again from zero. As we know the exact timing between each two increments of the timer contents, timer can be used for measuring time which is very useful with some devices.

CENTRAL PROCESSING UNIT has a role of connective element between other blocks in the microcontroller. It coordinates the works of other blocks and executes the user program.[5]

3.5 Clock / instruction cycle

Clock is microcontroller's main st component called an "oscillator" microcontroller with. If a time clock, our "clock" would then clock. In that case, oscillator could be compared to a spring that is would so time clock can run. Also, force used to win the time clock can be compared to an electrical supply.

Clock from the oscillator enters a microcontroller via OSCI pin where internal circuit of a

microcontroller divides the clock into four even clocks Q1, Q2, Q3 and Q4 which do not overlap. These four clocks make up one instruction cycle (also called machine cycle) during which one instruction is executed.[6]

3.6 RISC microprocessors

The high performance of the PIC micro devices can be attributed to a number of architectural features commonly found in RISC microprocessors. These include:

   i.   Harvard architecture

  ii.   Long Word Instructions

 iii.   Single Word Instructions

 iv.   Single Cycle Instructions

  v.   Instruction Pipelining

 vi.   Reduced Instruction Set

vii.   Register File Architecture

viii.   Orthogonal (Symmetric) Instructions

Harvard Architecture

Harvard architecture has the program memory and data memory as separate memories and is accessed from separate buses. This improves bandwidth over traditional von Neumann architecture in which program and data are fetched from the same memory using the same bus. To execute an instruction, a von Neumann machine must make one or more (generally more) accesses across the 8-bit bus to fetch the instruction.

Then data may need to be fetched, operated on, and possibly written. As can be seen from this description, that bus can be extremely congested. While with Harvard architecture, the instruction is fetched in a single instruction cycle (all 14-bits).While the program memory is being accessed, the data memory is on an independent bus and can be read and written. These separated buses allow one instruction to execute while the next instruction is fetched.[3]

Instruction Flow/Pipelining

An "Instruction Cycle" consists of Fetch takes one instruction cycle while decode and execute takes another instruction cycle. However, due to Pipelining, each instruction effectively
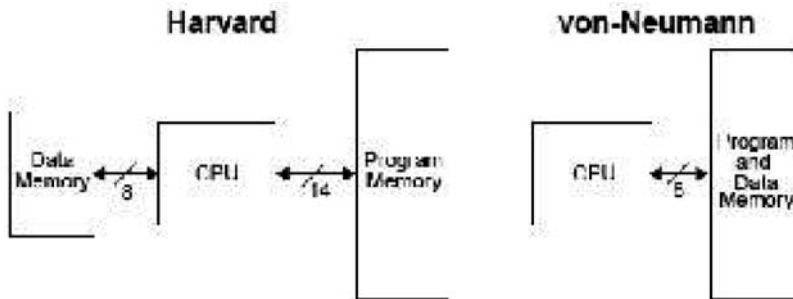
Figure 3.6.1: Harvard Vs. Von-Neumann block architecture

executes in one cycle. If an instruction causes the program counter to change (e.g .GOTO) then an extra cycle is required to complete the instruction. The instruction **fetch** begins with the program counter incrementing in Q1.

In the **Execution** cycle, the fetched instruction is latched into the "Instruction Register (IR)" in cycle executed during the Q2, Q3, and Q4 cycles. Data memory is read during Q2 (operand read) and written during Q4 (destinations write).

Example shows the operation of the two stage pipeline for the instruction sequence shown. At time T CY 0, the first instruction is fetched from program memory. During T CY 1, the first instruction executes while the second instruction is fetched. During T CY 2, the second instruction executes while the third instruction is fetched. During T CY 3, the fourth instruction is fetched while the third instruction (CALL SUB_1) is executed. When the third instruction completes execution, the CPU forces the address of instruction four onto the Stack and then changes the Program Counter(PC) to the address of SUB_1.[6]
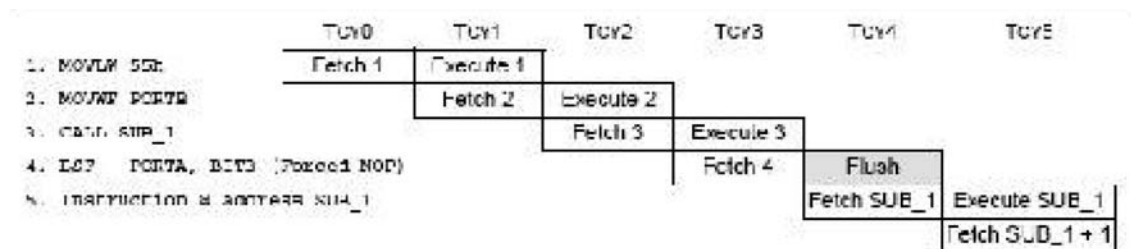
All instructions are single cycle, except for any program branches. These take two cycles since the fetch instruction is "flushed" from the pipeline while the new instruction is being fetched and then executed

Figure 3.6.2: Instruction Pipeline flow

Input output lines

General purpose I/O pins can be considered the simplest of peripherals. They allow the PICmicro to monitor and control other devices. To add flexibility and functionality to a device, some pins are multiplexed with an alternate function(s). These functions depend on which peripheral features are on the device. In general, when a peripheral is functioning, that pin may not be used as a general purpose I/O pin.
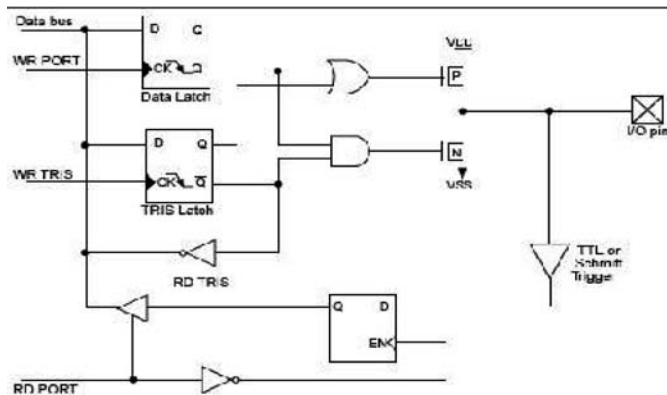
Figure 3.6.3 Logical gates

The direction of the I/O pins (input or output) is controlled by the data direction register, called the TRIS register. TRIS<x> controls the direction of PORT<x>. A '1' in the TRIS bit corres '0' corresponds to that pin being and the PORT register is the latch for the data to be output. When the PORT is read, the device reads the levels present on the I/O pins (not the latch). This means that care should be taken with read-modify-write commands on the ports and changing the direction of a pin from an input to an output.

Figure shows a typical I/O port. This does not take into account peripheral functions that maybe multiplexed onto the I/O pin. Reading the PORT register reads the status of the pins whereas writing to it will write to the port latch. All write operations (such as BSF and BCF instructions) are read-modify-write operations. Therefore a write to a port implies that the port pins are read; this value is modified, and then written to the port data latch.[4]

Regulated Power Supply

A **regulated power supply** is an embedded circuit, or standalone unit, the function of which is to supply a stable voltage (or less often current), to a circuit or device that must be operated within certain power supply limits. The output from the regulated power supply may be alternating or unidirectional, but is nearly always DC.[3]

The type of stabilization used may be restricted to ensuring that the output remains within certain limits under various load conditions, or it may also include compensation for variations in its own supply source.

3.7 MOTOR DRIVERS

D.C. Motor

A DC motor uses electrical energy to produce mechanical energy, very typically through the interaction of magnetic fields and current-carrying conductors.

The reverse process, producing electrical energy from mechanical energy, is accomplished by an alternator, generator or dynamo. Many types of electric motors can be run as generators, and vice versa. The input of a DC motor is current/voltage and its output is torque (speed).

The DC motor has two basic parts: the rotating part that is called the armature and the stationary part that includes coils of wire called the field coils. The stationary part is also called the stator.

Figure 3.7.1: DC motor

Figure shows a picture of a typical DC motor, Figure shows a picture of a DC armature, and Fig shows a picture of a typical stator. From the picture you can see the armature is made of coils of wire wrapped around the core, and core has an extended shaft that rotates on bearings. You should also notice that the ends of each coil of wire on the armature are terminated at one end of the armature. The termination points are called the commentator, and this is where the brushes make electrical contact to bring electrical current from the stationary part to the rotating part of the machine.[5]

Operation

The DC motor you will find in modem industrial applications operates very similarly to the simple DC motor described earlier in the chapter. The DC voltage is applied directly to the field winding and the brushes. The armature and the field are both shown as a coil of wire. In later diagrams, a field resistor will be added in series with the field to control the motor speed.

When voltage is applied to the motor, current begins to flow through the field coil from the negative terminal to the positive terminal. This sets up a strong magnetic field in the field winding. Current also begins to flow through the brushes into a commentator segment and then through an armature coil. The current continues to flow through the coil back to the brush that is attached to other end of the coil and returns to the DC power source. The current flowing in the armature coil sets up a strong magnetic field in the armature. [7]
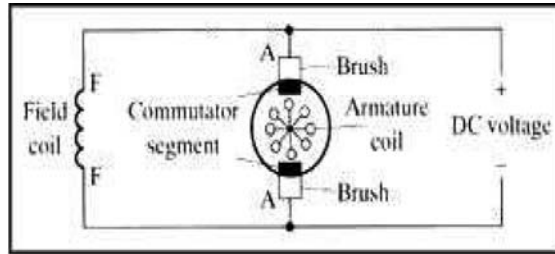
Figure 3.7.2: Simple electrical diagram of DC motor
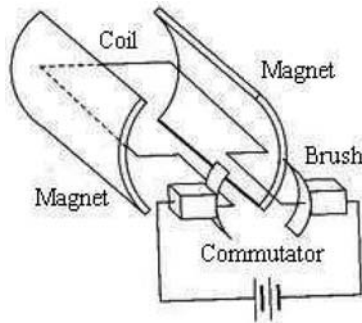
Figure 3.7.3: Operation of DC motor

The magnetic field in the armature and field coil causes the armature to begin to rotate. This occurs by the unlike magnetic poles attracting each other and the like magnetic poles repelling each other. As the armature begins to rotate, the commutator segments will also begin to move under the brushes. As an individual commutator segment moves under the brush connected to positive voltage, it will become positive, and when it moves under a brush connected to negative voltage it will become negative. In this way, the commutator segments continually change polarity from positive to negative.

Stepper Motor

Often a mechanical operation or function is required in an application. This may in turn require a motor or other mechanical device to position a load or device. While a conventional DC or AC motor can be used, it is difficult to accurately determine the exact position of the load, motor speed, or how much total motion has been produced, unless external positioning sensors, encoders, servo loops, and controlling devices (brakes, clutches, etc) are used.

Stepper Motor Driver

The stepper motor driver ULN2003A/L and ULN2023A/L have series input resistors
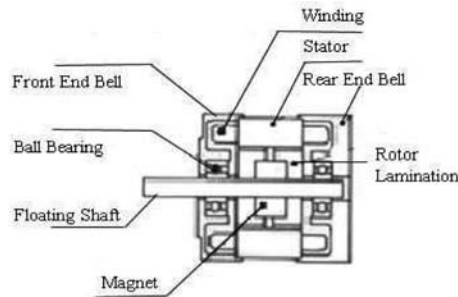
Figure 3.7.4: Stepper motor

selected for operation directly with 5 V TTL or CMOS. These devices will handle numerous interface needs - particularly those beyond the capabilities of standard logic buffers. The ULN2003A/L and ULN2004A/L are the standard Darlington arrays. The outputs are capable of sinking 500mA and will withstand at least 50 V in the OFF state. Outputs may be paralleled for higher load current capability. The ULN2023A/L and ULN2024A/L will withstand 95 V in the OFF state. These Darlington arrays are furnished in 16-pin dual in-line asdic packages -lead(suffix surface-mountable "A")

3.8   RS 232 & MAX 232

In telecommunications, **RS-232** is the traditional name for a series of standards for serial binary single-ended data and control signals connecting between a DTE (data terminal equipment) and a DCE (data circuit-terminating equipment). It is commonly used in computer serial ports. The standard defines the electrical characteristics and timing of signals, the meaning of signals, and the physical size and pinout of connectors. The current version of the standard is TIA-232-F Interface Between Data Terminal Equipment and Data Circuit-Terminating Equipment Employing Serial Binary Data Interchange, issued in 1997.

Many modern personal computers have no RS-232 ports and must use an external USB-to-RS-232 converter to connect to RS-232 peripherals. RS-232 devices are still found, especially in industrial machines, networking equipment, or scientific instruments.[8]

RS-232 stands for Recommend Standard number 232 and C is the latest revision of the standard. The serial ports on most computers use a subset of the RS-232C standard. The full RS-232C standard specifies a 25-pin "D" connector of which 22 pins are used. Most of these pins are not needed for normal PC communications, and indeed, most new PCs are equipped with male D type connectors having only 9 pins. The details of RS232 are as shown in table.

MAX 232

The MAX232 is a dual driver/receiver that includes a capacitive voltage generator to supply TIA/EIA-232-F voltage levels from a single 5-V supply. Each receiver converts TIA/EIA-232-F inputs to 5-V TTL/CMOS levels. These receivers have a typical threshold of 1.3 V, a typical hysteresis of 0.5 V, and can accept ±30-V inputs. Each driver converts TTL/CMOS input levels into TIA/EIA-232-F levels.[1]
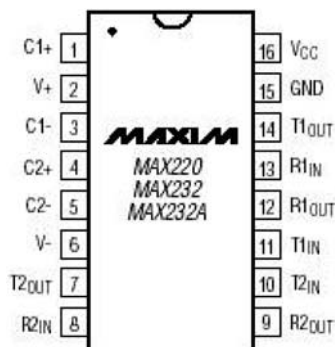
Figure 3.8.1: Pin out diagram of max 232

3.9 Zigbee transceiver

ZigBee is a specification for a suite of high level communication protocols using small, low-power digital radios based on an IEEE 802 standard for personal area networks. ZigBee devices are often used in mesh network form to transmit data over longer distances, passing data through intermediate devices to reach more distant ones. This allows ZigBee networks to be formed ad-hoc, with no centralized control or high-power transmitter/receiver able to reach all of the devices. Any ZigBee device can be tasked with running the network.[1]

ZigBee is targeted at applications that require a low data rate, long battery life, and secure networking. ZigBee has a defined rate of 250 kbit/s, best suited for periodic or intermittent data or a single signal transmission from a sensor or input device. Applications include wireless light switches, electrical meters with in-home-displays, traffic management systems, and other consumer and industrial equipment that requires short-range wireless transfer of data at relatively low rates. The technology defined by the ZigBee specification is intended to be simpler and less expensive than other WPANs, such as Bluetooth or Wi-Fi.

CC2500 Serial Transceiver Wireless Module is designed to meet the requirement for the low cost, low power wireless device to transmit and receive serial data. The module operates on 2.4 GHz frequency band. The module can also be used as Wireless Sensor Network (WSN) node.

3.10 Working

The module has **simple Protocol** for working. the Using CC transreceiver GUI, the module can be configured data communication through hyperterminal. This modules basically take **TTL data & send it to receiver** (receiver whose ID is send along with data). Modules can also broadcast the data (broadcast id (0xff).A single module can communicate with number of modules at run time. as receiver ID needs to send every time, So one can send different receiver id every time to communicate with different modules. This feature makes it best suited for swarm robotics. As modules has capability of analog to digital conversion (ADC). So user has to just configure the module once for ADC, & the module will send the data to the respective receiver, at the given interval of time.

Pin connections

CC2500 transceiver module is having 3 connector headers (P1, P2 & P3as shown in picture). P1 is having 4 pins GND (V-), VCC (V+), Rx, Tx. Where Jumper 2 is having 6 pins A0 to A5 (ADC 0 to ADC 5). [2]

Configuring CC2500 Module

CC2500 module can configure for various things like Self ID (self-address or SID), Channel ID (CID), Baud Rate (max 38400bps) and ADC values.

Configuring Self ID & Channel ID

CC2500 module can be configured by various ways. It can configure during use through programming, HyperTerminal Or through CC2500 wireless GUI. To configure the module we need to follow some protocol (some set of commands). Protocol for configuring self ID & channel ID is given below. In which we have to give Self ID / Self Address (range 0 to 255 in decimal 0R 0x00 to 0xFF in Hex) and channel ID / Channel Address (range 0 to 255 in decimal 0R 0x00 to 0xFF in Hex). It is to be noted that the Self ID 0xFF (in hex) Or 255 (in decimal) is reserved for broadcast. Protocol for configure self-ID & Channel ID.

"< Self_id >" Channel_id

Configuring Baud rate

CC2500 module can support for different baud rates. Modules can be configured for different baud rate (default is 9600 bps) using simple Protocol or it can be done using GUI. Protocol for configuring Baud rate includes Baud rate index (1-3). Sending this baud rate index can change

its own baud rate. It is to be noted that changing a baud rate may leads to failure after configuration. So one has to change the baud rate of other device also.Protocol for configuring Baud rate is

"(Baud rate   index)"

3.11 Wireless A/V Camera

Figure 3.11.1: Camera with AV receiver

Wireless cameras are the security system of choice, taking into account that wireless cameras are not limited by conventional boundaries. Wireless security at home or office is a paramount issue with the economy as it is. Safety and assets are becoming more and more vulnerable, and the industry is striving to keep up with the demands for flexibility, versatility and mobility. Airtight Security Plus can help; call one of our specialists for a one on one conversation.

Wireless range

Wireless security cameras function best when there is a clear line of sight between the camera(s) and the receiver. Outdoors, and with clear line of sight, digital wireless cameras typically have a range between 250 to 450 feet. Indoors, the range can be limited to 100 to 150 feet. The signal range varies depending on the type of building materials and/or objects the wireless signal must pass through.

Uses and Applications

Wireless security cameras are becoming more and more popular in the consumer market. They are a cost-effective way to have a comprehensive surveillance system in your home or business without needing an expensive installation.

Wireless cameras are also a great for people renting homes or apartments. Since there is no need to run video extension cables through walls or ceilings (from the camera to the receiver or recording device) one does not need approval of a landlord to install a wireless security camera system.

A wireless security camera is also a great option for seasonal monitoring and surveillance. You can observe your pool or patio in the summer months and take down the camera in the winter.

Pros

i. Affordable: the cost of individual cameras is low

ii. Multiple receivers per camera: the signal from one camera can be picked up by any receiver; you can have multiple receivers in various locations to create your wireless surveillance network

Cons

i. Susceptible to interference from other household devices, such as microwaves, cordless phones, video game controllers, and routers

ii. Signal is not secure—neighbours can pick up the transmission on their radios or other devices on a similar bandwidth.

iii. Quality of video and audio is average/poor; image can degrade significantly with inter-ference[6]

4 Sensors

4.1 CO_2 Sensor

Figure 4.1.1: CO_2 sensor

The sensing element of Figaro gas sensors is a tin dioxide (Sn02) semiconductor which has low conductivity in clean air. In the presence of a detectable gas, the sensors conductivity increases depending on the gas concentration in the air. A simple electrical circuit can convert the change in conductivity to an output signal which corresponds to the gas concentration.

The figure below represents typical sensitivity char-acteristics, all data having been gathered at standard test conditions (see reverse side of this sheet). The Y-axis is indicated as sensor resistance ratio (RsIRo) which is defined as follows:

Rs = Sensor resistance of displayed gases at various concentrations

Ro = Sensor resistance in l000ppm methane

The figure below represents typical temperature and humidity dependency characteristics. Again, the Y-axis is indicated as sensor resistance ratio (Rs/Ro), defined as follows:

Rs = Sensor resistance at l000ppm of methane at various temperatures/humidity's

Ro = Sensor resistance at l000ppm of methane at 20°C and 65% R.H.

4.2 Structure and Dimensions
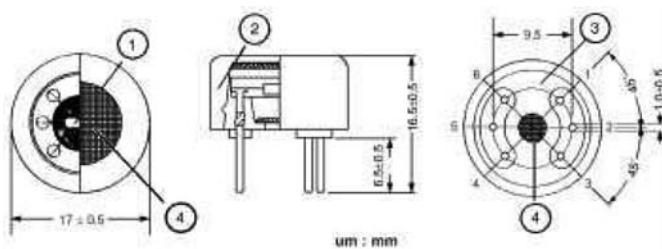
Figure 4.2.1: Structural Diagram of CO_2 sensor

Pin Connection and Basic Measuring Circuit

The numbers shown around the sensor symbol in the circuit diagram at the right correspond with the pin numbers shown in the sensors structure drawing (above). When the sensor is connected as shown in the basic circuit, output across the Load Resistor (VRL) increases as the sensors resistance (Rs) decreases, depending on gas concentration.(4)

Standard Test Conditions

TGS 813 complies with the above electrical characteristics when the sensor is tested in standard conditions as specified below:

Test Gas Conditions: 20°±2°C, 65±5%R.H.

Circuit Conditions: Vc = 10.0±0.1V (AC or DC), VH = 5.0±0.05V (AC or DC),

RL = 4.OkQ±1%(4)

Preheating period before testing: More than 7 days

Sensor Resistance (Rs) is calculated by the following formula

$$Rs = \left(\frac{Vc}{V_{RL}} - 1 \right) \times RL$$

Power dissipation across sensor electrodes (Ps) is calculated by the following formula

$$Ps = \frac{Vc^2 \times Rs}{(Rs + RL)^2}$$

Temperature Sensor

The LM35 series are precision integrated circuit temperature sensors, whose output voltage is linearly proportional to the Celsius (centigrade) temperature. The LM35 thus has an advantage over linear temperature sensors calibrated in Kelvin as the user is not required to subtract a large constant voltage from its output to obtain convert centigrade scaling.

The LM35 does not require any external calibration or trimming to provide typical accuracy'satroomtemperatureofand$\pm1/4\pm3/4$°cover°ca full -55 to +150 °c temperature range. Trimming and calibration at the wafer level assure low cost. The Lm35's l precise inherent calibration makes interfacing to readout or control circuitry especially easy. It can be used with single power supplies, or with pulse and minus supplies.

As it draws only 60microamp from its supply, it has very low self-heating, less than 0.1c in still air. The LM35 is rated to operate over a-55 to 150-°c-temperature range while the LM35cis rated for a -40 to +110 °c (-10 with improved accuracy).

4.3 MP Lab

MP Lab is software used where the machine code is written and compiled. After compilation the machine code is converted into hexadecimal code which is to be dumped into the microcontroller for further processing. MP Lab also supports C language code. It's important that you know C lan commonly known as Embedded C. the PCB, PCM and PCH are separate compilers. PCB is for 12-bit opcodes. PCM is for 14-bit opcodes, and PCH is for 16-bit opcode PIC microcontrollers. Due to many similarities, all these three compilers are covered in this reference manual.[5]

#include<16F877A.h> // header file for PIC 16F877A//

5. Result

The paper "PC   Controlled Wireless Robot" can move either forward by pressing button ' button 'I', left by pressing button '.

The stepper motor for the rotatable camera can be turned in clockwise direction by pressing button I -clockwise direction 'A' and by pressing button 'B' from the PC RF communication.

6. Conclusion

The PC controlled wireless robot is completely assembled with four DC motors for its movement and the sensors are fixed to sense the temperature and CO_2 gas. The stepper motor controlled with the stepper motor driver is connected with the wireless camera for the rotation purpose. All the components are connected with the microcontroller for control by the user.

Integrating features of all the hardware components used have been developed in it. Presence of every module has been reasoned out and placed carefully, thus contributing to the best working of the unit. Secondly, using advanced IC's with the help of growing successfully implemented.

References

1. Drew Gislason (via EETimes), "ZigBee Wireless Networking",

2. F. Egan, William (2003), Practical RF System Design. Wiley-IEEE Press. ISBN 978-0-471-20023-9.

3. Heath, Steve (2003), Embedded systems design. EDN series for design engineers (2 ed.). Newnes. p. 2. ISBN 978-0-7506-5546-0.

4. Odd Jostein Svendsli 2003, "Atmel's-ProgrammingSelfFlash Microcontrollers".

5. Vasile Tompa and Dan Hurgoiu, "Remot Autonomous Mobile Robot", Technical-Napoca, Romania Univers.

6. IEEE Standards 802.15.4, IEEE 2003, ISBN 0-7381-3677-5 SS95127.

SHORT TERM EFFECT ON COMPOSTED COIR PITH, FARMYARD MANURE AND VERMI COMPOST ON THE PHYSICAL AND CHEMICAL PROPERTIES OF THE SOIL WITH THE YIELD OF PEARL MILLET

F.Jeyamangalam and P.Jeyalakshmi

Abstract

This experiment was conducted at Perumalpuram of Tirunelveli District of Tamil Nadu, South India to evaluate the effect of different organic manures and their combinations on various physical, chemical and physico-chemical properties of the soil and their impact on Pearl millet. The treatments of this study were Composted coir pith (CP), Farmyard manure (F) and Vermicompost (VC). The above manures were applied and after 30 days, the soil was collected in each sample area and analyzed. Pearl millets were grown and again soil samples were analyzed after the harvest of the crop. The yield was high as 4953 kg ha^{-1} with the combinations of VC+F in equal combinations @ 12.5 t ha^{-1} where as the control area had 2791 kg ha^{-1}. The Bulk density (BD), Particle density (PD), pH and Electrical Conductivity (EC), had decreased in all the combinations other than control. Percentage of Water Holding Capacity (WHC), Pore Space (PS), Saturated Moisture (SM) and NPK content, had increased. Thus applications of amendments in the proper combinations may be a good strategy to reclaim the low nutrient soils.

Keywords

Composted coir pith, Farm yard manure, vermicompost, amendments, and physical properties.

Introduction

Pearl millet (*Pennisetum glaucum*) is a staple food in India, particularly in the states of Rajasthan, Gujarat, and Maharashtra. (Velu *et al*., 2008). Pearl millet is well adapted to growing areas characterized by drought, low soil fertility, and high temperature. It performs well in soils with high salinity or low pH. Pearl millet is one of the most extensively cultivated cereals in the

Department of physics, Sarah Tucker College, Tirunelveli, Tamil Nadu, India.

Email: f.jeyamangalam@yahoo.com

world, after rice, wheat, and sorghum, and particularly in arid to semi-arid regions. India is the largest producer of pearl millet. Rajasthan is the highest producing state in India. Pearl millet is an important food across India.

Worldwide, especially in organic and sustainable agriculture, manure is used as a source of organic matter (OM) to improve soil quality as well as the traditional source of crop nutrients (Kumar *et al.*, 2006). Soil quality and good soil management are vital components of sustainable crop production because soil supports the fundamental physical, chemical, and biological processes that must take place in order to support plant growth.

Materials and Methods

This experiment was carried out at Perumalpuram of Tirunelveli district of Tamilnadu, South India in 2015.It is located at $8.689^{\%}$ latitude and $77.738^{\%}$ longitude.

The control sample was obtained as fine tilt without stubbles and weeds. While adding organic manure, care was taken to see that the individual treatments were mixed separately. Each sample was left without any disturbance and the experimental soil was levelled perfectly for uniform application. By using different organic manures of F, CP, and VC in different concentrations (7.5t ha^{-1}, 12.5t ha^{-1} and 17.5t ha^{-1}) the total treatment consists of 22 samples including control plot. The pod yield in each sample was measured.

1. Physical Properties

1.1. Bulk Density (BD)

Bulk density is defined as the mass (weight) per unit volume of a dry soil (volume of solid and pore spaces). It is expressed in gm cm^{-3}. Generally, in normal soils bulk density ranges from 1 – 1.60 gm cm^{-3}.

1.2. Particle Density (PD)

The weight per unit volume of the solid portion of soil is called particle density.   It is also termed true density which is expressed in gm cm^{-3}. Generally, in the normal soils the particle density is 2.65 gm cm^{-3}.

1.3. Water Holding Capacity (WHC)

Water holding capacity is defined as the capacity of the soil to retain water is exceeded. At this point all soil pore spaces (micro and macro pore spaces) are filled up with water and the drainage is restricted.

1.4. Pore Space (PS)

Pore spaces (also called voids) in a soil consist of the portion of the soil volume not occupied by solids, either mineral or organic. The pore space under field conditions is occupied at all times by air and water. Pore spaces directly control the amount of water and air in the soil and indirectly influence the plant growth and crop production.

1.5. Saturated Moisture (SM)

At soil saturation, water fills completely in the pore spaces.

2. Chemical Properties

2.1. Available Nitrogen (N)

The amount of nitrogen released by oxidizing a portion of soil organic matter using alkaline $KMnO_4$ is estimated by distillation with NaOH. The distillate is collected in boric acid containing double indicator and titrated against standard H_2SO_4, (Subbiah and Asija, 1935).

2.2. Available Phosphorus (P)

Phosphorus is present in soil as calcium phosphate, iron and aluminium phosphate, organic phosphate etc. Only a small fraction of these phosphates is available to crops. For extraction of available P in normal soils, the Olsen's method (Olsen *et al.*, 1954) is used. The phosphorus of the solution is measured using a spectrophotometer at 660 nm.

2.3. Available Potassium (K)

Potassium in soil occurs as water soluble K, exchangeable K, non-exchangeable K and mineral K. Out of these fractions, water soluble K and exchangeable K fractions are called as available K. The available K can be extracted using neutral normal ammonium acetate solution in a soil to solution ratio of 1:5. The available K in the extract is estimated using flame photometer (Handway and Heidel, 1952).

3.Physico-Chemical Properties

3.1. Electrical Conductivity (EC)

The EC of soil indicates the total amount of soluble salts present in the soil solution and is expressed as ds m^{-1} (deci siemens per meter). When a soil contains excess amount of soluble salts, it is termed as saline soil. In saline soils, the crop growth is restricted due to high soil water potential (osmotic potential). EC is measured in terms of resistance offered to the flow of current using a conductivity meter (Jackson, 1973).

3.2. Determination of Soil pH

The term pH (Puissance de Hydrogen) was introduced by Sorenson in 1909 to express hydrogen ion concentration in water and water based solutions. pH is defined as "the negative logarithm (base 10) of hydrogen ion activity" $pH = \log_{10} 1/[H+] = - \log_{10} [H+]$

The physical properties like BD, PD, WHC, PS and SM were analyzed by Keen Raczkowski (KR) box given by Keen *et al.,* (1921). The data were statistically analyzed using analysis of variance (ANOVA) as applicable to complete the randomized block design, and least significant difference (LSD) at $P = 0.05$ was used to test the differences between means of individual treatments (Gomez and Gomez, 1984).

Research Findings And Analysis

1. Physical Properties

BD: Bulk density decreased positively with increasing organic matter source such as vermicompost. The maximum value (1.534gm cm^{-3}) was seen in the control plot as shown in Table 1. After different combination of organic amendments the bulk density has decreased till 1.015 gm cm^{-3} with the combination of VC+F @ 12.5 t ha^{-1}. This is in line with the findings of Shirani *et al*., (2002), who revealed that the effect of balanced fertilizer and VC manure application on bulk density of the surface soil (0-15 cm) was significant.

PD: The decrease in PD from the control was obvious with incorporation of organic manure. PD was the lowest as 1.708 gm cm^{-3} @ 17.5t ha^{-1} with VC. PD was the highest in control plot and with the amendment of manures; PD values have decreased to the greater extent.   Similar results were revealed by the studies of Melis *et al*., (2008) using composted tobacco waste and farm yard manure.

WHC: Water holding capacity was increased due to the addition of organic manure. In VC+CP+F amended plot WHC increased as 44.92, 50.79 and 56.73% for plots with organic manure @ 7.5, 12.5 and 17.5 t ha^{-1} respectively and the control had the value of 28.42%. Similar results were obtained by Dong *et al*., (2006).

PS: The pore space was increased as 40.95, 47.15 and 54.31% in VC + CP amended plot @ 7.5, 12.5 and 17.5t ha^{-1} respectively. PS was the maximum as 54.54% in VC plot @ 7.5 t ha^{-1} which was higher than the control with 27.65%. According to Jeyamangalam (2015) the increase of 14.89% than control was noticed in the F+CP+TS plot @ 12.5 t ha^{-1}.

Table 1. Physical properties of organically amended soil before harvest

S.NO	MANURE	SAMPLE	BD gm cm^{-3}	PD gm cm^{-3}	WHC %	PS %	SM %
1	VC	T3A	1.054a	2.295	49.21d	54.54a	37.89e
2	VC	T3B	1.072a	1.943	53.10b	46.34cd	48.69a
3	VC	T3C	1.121ab	1.708	47.06e	35.21g	40.60c
4	VC+CP	T5A	1.256bc	2.014	40.08g	40.95f	31.98g
5	VC+CP	T5B	1.132ab	1.910	41.90g	47.15c	39.98d
6	VC+CP	T5C	1.223bc	2.325	47.21e	54.31a	36.07
7	VC+F	T6A	1.404de	2.042	40.83g	33.10h	36.01ef
8	VC+F	T6B	1.015a	1.969	46.57e	42.91e	35.21f
9	VC+F	T6C	1.385cd	2.626	32.05h	47.87bc	27.27h
10	VC+CP+F	T7A	1.053a	2.461	44.92f	53.25a	34.52f
11	VC+CP+F	T7B	1.155ab	2.070	50.79c	49.27b	45.76b
12	VC+CP+F	T7C	1.313cd	1.821	56.73a	45.10d	47.18a
13	CONTROL	T8	1.534e	2.819	28.42i	27.65i	24.73i
Grand mean			1.2186	2.1100	44.5723	44.4854	37.3049
Significance			**	NS	**	**	**
SEd			0.0706	0.4638	0.7480	0.7294	1.0269
CD (0.05)			0.1456	0.9572	1.5437	1.5055	2.1195
CV (%)			7.09	26.92	2.06	2.01	3.37

VC-Vermicompost   CP-Composted coir pith   F-Farmyard manure

A-7.5 t ha^{-1} B-12.5 t ha^{-1} C-17.5 t ha^{-1}

BD-Bulk Density   PD-Particle Density   WHC- Water Holding Capacity

SM-Saturated Moisture   PS-Pore Space

SM: It is a property which is endowed with the ability to retain soil moisture. The slow release in moisture enhances crop yields. It has the maximum as 48.69% in VC amended plot @ 12.5 t ha^{-1}. SM was the lowest in the control plot with the value 24.73%.

Table 2. Chemical & Physico-chemical properties of organically amended soil before harvest

S.NO	MANURE	SAMPLE	N kgha⁻¹	P kgha⁻¹	K kgha⁻¹	pH	EC dsm⁻¹	YIELD Kg ha⁻¹
1	VC	T3-A	104 de	64 g	500 a	8.2	0.18 bcd	3341
2	VC	T3-B	130 b	106 c	500 a	8.2	0.22 def	4481
3	VC	T3-C	154 a	98 d	240 e	8.2	0.26 fg	3145
4	VC+CP	T5-A	95 f	54 h	153 h	8.1	0.19 cde	3459
5	VC+CP	T5-B	96 f	47 i	225 f	8.2	0.13 ab	3656
6	VC+CP	T5-C	105 d	82 e	132 i	8.2	0.14 ab	3852
7	VC+F	T6-A	109 d	59 g	500 a	8.2	0.14 ab	3341
8	VC+F	T6-B	126 b	123 a	270 d	7.9	0.24 efg	4953
9	VC+F	T6-C	156 a	72 f	189 g	8.1	0.11 a	4285
10	VC+F+CP	T7-A	99 ef	26 j	285 c	8.1	0.15 abc	3333
11	VC+F+CP	T7-B	104 de	64 g	135 i	7.9	0.25 fg	3727
12	VC+F+CP	T7-C	116 c	117 b	400 b	7.8	0.24 fg	4010
13	CONTROL	T8	87 g	11 k	122 j	8.3	0.28 g	2791
Grand mean			113.8974	71.0256	280.7949	8.1179	0.1949	3701.58
Significance			**	**	**	NS	**	**
SEd			2.5428	2.3473	2.5307	0.2232	0.0254	7.0912
CD (0.05)			5.2481	4.8447	5.2232	0.4606	0.0524	200.387
CV (%)			2.73	4.05	1.10	3.37	15.96	3.21

VC- Vermicompost   CP- Composted coir pith   F - Farm Yard Manure

A - 7.5t ha⁻¹   B - 12.5t ha⁻¹   C - 17.5t ha⁻¹

N - Nitrogen   P -phosphorus   K - Potassium

EC - Electrical Conductivity

2. Chemical Properties

N: The N content increased as concentration of the organic manure increased. This was noticed in the vermicompost amended plot as the dosage of organic manure increased @ 7.5, 12.5 and 17.5 t ha^{-1}, the value of N content increased as 104, 130 and 154 kg ha^{-1} respectively as shown in Table 2. It was 44% higher than control plot. The higher nitrogen content contributed to greater height of the plant (Sharma and Dayal, 2005).

P: The level of the phosphorous (P) content was maximum as 123 kg ha^{-1} in VC+F plot @ 12.5 t ha^{-1}. It was 91% higher than control plot which is minimum as 11kg ha^{-1}. This is similar to the result of Nethra *et al.,* (1999).

K: The value of potassium was high as 500 kg ha^{-1} in VC @ 7.5 t ha^{-1}. The lowest value 122 kg ha^{-1} was recorded in the control plot. The maximum value of K was 75 % higher than control plot. The present results were in accordance with Mohankumar and Naresh Gowda (2010).

3. Physico-Chemical Properties

EC: The EC of the soil has considerably reduced in all the plots. The EC of the soil amended with VC had the decreased values compared to the control plot. In the present study the value of EC was the lowest (0.11 ds m^{-1}) in the treatment of VC+F @ 17.5 t ha^{-1}. It was 60% lower than control plot at 0.28 ds m^{-1}. The similar effect of soil pH has been reported by Srikanth *et al.,* (2003) which could be described as the effect of organic acids produced during the decomposition.

pH: In the present study for VC+F+CP plot @ 17.5 t ha^{-1} the value of pH was minimum with value 7.8 which was 6% lower than control plot. The control plot had 8.3 which was the maximum value. This is possible during microbial decomposition organic manure. Organic acid may have been released, which neutralized the alkalinity of the organic manures thereby leaving the pH of the soil almost what it was initially which is favourable for a good crop production as revealed by Okwuagwu *et al.,* (2003).

Yield: The Yield was maximum as 4953 kg ha^{-1}, the most superior treatment with equal combination of F+VC @ 12.5 t ha^{-1} as shown in fig.1. The control yielded 2791 kg ha^{-1}. It is an unusually hardy food crop, and consequently there is a progressive increase in the use of these grains as a major food staple, especially among subsistence farmers and the rural poor in large areas of India and sub-Saharan Africa (Vom Brocke *et al*., 2012).
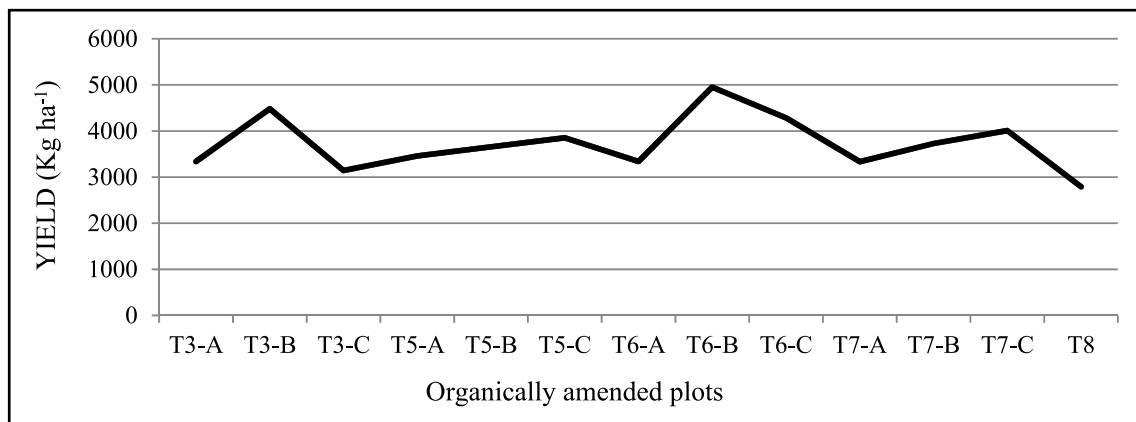
Fig. 1 : Yield of pearl millet in organically amended plot

Conclusion

It is concluded that, for the improvement of low nutrient soils, recycled organic wastes have various positive effects on soil attributes and increased yield of pearl millet pods. Considering the salient findings, perspective organic farming favourably influenced the soil physical, chemical and physico-chemical properties of the soil which in turn paved way for better crop yield and quality. Thus, application of organic amendments in the proper combination may be a good strategy to reclaim the soils.

References

1. Dong, J., Hengsdijk, H., Dai, Ting-Bo, De Boer, W., Jing, Q. and Wei-xing Cao (2006). Long-term effects of manure and inorganic fertilizers on yield and soil fertility for a winter wheat-maize system in Jiangsu, China. *Pedosphere*, **16(1)**: 25-32.

2. Gomez, K.A. and Gomez, A.A. (1984).Statistical procedures for agricultural research. New York: Wiley Inter Science, 2nd edn., P 95-109.

3. Hanway, J.J. and Heidal, H. (1952). Soil analysis methods as used in lowa State College, Soil Testing Laboratory. *Lowa Agriculture.*, **57**:1-31.

4. Jackson,M.L., (1973). Soil Chemical Analysis, Prentice Hall, New Delhi, *1st edn.,* 89-91.

5. Jeyamangalam, F. (2015). Effect of organic manure in controlling environmental pollution.*Journal of Modern Science*, **7(2)**: 20-26.

6. Keen, B.A. and Raczkowski, H. (1921). Relation between the clay content and certain physical properties of a soil. *Journal of Agricultural Science,***11**: 441-449.

7. Kumar, K., Gupta, S.C., Baidoo, S.K., Chander, Y. and Rosen. C.J. (2006). Antibiotic uptake by plants from soil fertilized with animal manure. *Journal of Environmental Quality* **34**:2082–2085.

8. Mohankumar, A.B. and Narase Gowda, N.C. (2010). Effect of different organic manures and inorganic fertilizers on available NPK, microbial density of the soil and nutrient uptake of brinjal (*Solanummelongena.L.*). *An Asian Journal of Soil Science,* **5**:291-294.

9. Melis Cercio Lu, Bulent Okur, Sezai Delibacak and Ali Riza Ongun (2008). Effects of composted tobacco waste and farmyard manure on some soil physical properties and lettuce yield. International meeting on soil fertility land management and Agroclimatology. Turkey, P:647-654.

10. Nethra, N. N., Jayaprasad K.V.,and Kale, K.V., (1999). China as ter (Callistephus chinensis L.) cultivation using vermicomposts as organic amendment, *Crop Research Hisar*., **17(2):** 209-215

11. Okwuagwu, M.I., Alleh, M.E. and Osemwota, I.O. (2003). The effects of organic and inorganic manure on soil properties ad yield of Okra in Nigeria. African Crop Science Conference Proceedings, **6**:390-393

12. Olsen, S.R., Cole, C.U., Watanable, F.S. and Deen, L.A. (1954). Estimation of available phosphorus in soil by extracting with sodium bicarbonate. USDA circular 939, Washington.

13. Sharma, V.K. and Dayal, B. (2005). Effect of organic and inorganic source of nitrogen on growth, yield and nutrient uptake under cowpea, linseed croppim]ng system. *Legume Research,* **28 (2):** 79-80.

14. Shirani, H., Ma Hajabbasi, Afyuni, M. and Hemmat, A. (2002). Effect of farm yard manure and tillage system on soil physical proportion and corn yield in central Iran. *Soil and Tillage Research*, **68**:101-108.

15. Srikanth, K.C., Srinivasamurthy, A., Siddaramappa, R. and Ramakrishnaparama, V.R., (2000). Direct and residual effects of enriched composts FYM, vermicompost and fertilizers on properties of an alfisol. *Journal of Indian Society of Soil Science,* **48**:494-499.

16. Subbaiah,B.V. and G.C,Asija (1956). A rapid procedure for determination of available nitrogen in soils. *Current Science,* **25**:259-260.

17. Velu, G., Rai, K.N. and Sahrawat, K.L.(2008) Variability for grain iron and zinc content in a diverse range of pearl millet populations. *Journal of Crop Improvements* **35**:186-91.

18. Vom Brocke, K., Haussmann BIG, Rattunde, F.H, Weltzien-Rattunde E, Traore PCS.and Parzies HK. (2012) Breeding Strategies for Adaptation of Pearl Millet and Sorghum to Climate Variability and Change in West Africa. *Journal of Agronomy and Crop Science,* **198:**327-39.

GENERALIZED PARIKH VECTORS OF ARRAYS

Huldah Samuel, Robinson Thamburaj, D. Gnanaraj Thomas

Abstract

The Parikh vector which plays a significant role in the field of Formal Language Theory gives the number of occurrences of each letter of the alphabet in the word. Motivated by this another measure called generalized Parikh vector (GPV) which reflects the positions of each letter of the alphabet was introduced by Siromoney et al.[6]. In this paper we introduce GPV for non-linear strings and arrays and study the properties of the same. Operators on GPV of words and their connection with circular languages are also dealt with.

1. Introduction

The classical Parikh mapping also called the Parikh vector, introduced in [3] is a significant contribution in the theory of formal languages. The Parikh vector of a word counts the number of occurrences of each letter of the alphabet. While Parikh mapping is defined for finite words, the measure of position vectors introduced by Siromoney et al. is defined for infinite words also. The position vector of an infinite word has a nice form and reflects the distinction between different infinite words and is called the generalized Parikh vector (GPV).

In this paper we have defined GPV for non-linear strings and arrays. GPVs of rectangular arrays, partial arrays, special types of arrays such as the triangular array, hexagonal array and polygonal array have been defined and a few properties have been studied.

2. Preliminaries

We recall some basic notations concerning words [2].

Department of Mathematics, Madras Christian College, Chennai - 600 059.

Definition 2.1. Let Σ be a finite non empty set of symbols called an alphabet. Symbols in Σ are called letters and any finite string over Σ is called a word over Σ. For a word w over Σ we write $|w|$ to indicate the length of w. If $|w| = \infty$, then w is called an infinite word. It is also known as ω-word. The empty word is denoted by λ. The set of all words over Σ is denoted by Σ^*.

Definition 2.2. Let $\Sigma = \{a_1, a_2, \ldots, a_n\}$. Then the Parikh image of a word u is given by $\pi(u) = (|u|_{a_1}, |u|_{a_2}, \ldots, |u|_{a_n})$ where $|u|_{a_i}$ represents the number of times a_i is occurs in u.

Definition 2.3. Let $x \in \Sigma^\infty$. The Generalized Parikh Vector (GPV) of x denoted by p(x) is $(p_1, p_2) \in [0, 1]^2$ where $p_1 = \sum_{j \in A_1} \frac{1}{2^j}$, $p_2 = \sum_{j \in A_2} \frac{1}{2^j}$, where A_1 and A_2 contain the positions of a and b in x, respectively. If $L \subseteq \Sigma^\infty$, let $p(L) = \{p(x) / x \in L\}$.

Example 2.1. If $\Sigma = \{a, b\}$ and u = aaba, then $p(u) = \left(\frac{1}{2} + \frac{1}{2^2} + \frac{1}{2^4}, \frac{1}{2^3} \right)$.

If $v = (ab)^\omega$, then $p(v) = \left(\frac{1}{2} + \frac{1}{2^3} + \frac{1}{2^5} + \Lambda , \frac{1}{2^2} + \frac{1}{2^4} + \frac{1}{2^6} + \Lambda \right) = \left(\frac{2}{3}, \frac{1}{3} \right)$.

Definition 2.4. A partial word x is defined as a partial function from $\{1, 2, \ldots, |x|\}$ to Σ. The positions where x(n), the nth letter of x, is not defined for $n < |x|$, are called holes of x. D(x) denotes the domain of x, and the set of all holes of x are denoted by H(x) where $H(x) = \{\{1, \ldots, |x|\} \setminus D(x)\}$.

Example 2.2. Let $x = ab\lozenge abb\lozenge ba$ be a partial word. Then $D(x) = \{1,2,4,5,6,8,9\}$ and $H(x) = \{3,7\}$.

A word over Σ is a partial word over Σ with an empty set of holes. The collection of all partial words is denoted by $\Sigma^*_\lozenge$. The symbol $\lozenge$ is used to represent a hole. For any partial word u over Σ, $|u|$ denotes its length including its holes. i.e., if $x = ab\lozenge abb\lozenge ba$ then $|x| = 9$. **Definition 2.5.** Let u be a partial word over Σ, where $\Sigma = \{a, b\}$. The Generalized Parikh Vector (GPV) of u is $P_\lozenge(u) = \left\{ (p_1, p_2) \in [0,1]^2, p_1 = \sum_{j \in A_1} \frac{1}{2^j}, p_2 = \sum_{j \in A_2} \frac{1}{2^j} \right\}$ where A_1 and A_2 denote the positions of a and b in u, where the positions representing the holes are neglected.

Definition 2.6. An array $A = (a_{ij})_{m \times n}$ over an alphabet Σ is a rectangular arrangement of symbols of Σ in m rows and n columns. The size of the array A is the ordered pair (m, n). The set of all arrays over Σ together with the empty array λ is denoted by Σ^{**} [1].

Definition 2.7. A partial array A of size (m, n) over Σ is a partial function $A : Z_m \times Z_n \to \Sigma$ where Z is the set of all positive integers. For $1 \le i \le m$, $1 \le j \le n$, if A(i, j) is defined then we say that (i, j) belongs to the domain A (denoted by $(i, j) \in D(A)$); otherwise, we say that (i, j) belongs to the set of holes of A (denoted by $(i, j) \in H(A)$). An array over Σ is a partial array over Σ with an empty set of holes.

Example 2.3.

$$A = \begin{array}{ccccc} b & \Diamond & a & \Diamond & b \\ \Diamond & a & \Diamond & b & \Diamond \\ a & b & a & \Diamond & b \end{array} \quad \text{is a partial array of size 3x5.}$$

D(A)={ (1,1),(1,3),(1,5),(2,2),(2,4),(3,1),(3,2),(3,3),(3,5).

3. GPV of Linear, Non-linear Strings and Array

Definition 3.1. Let $\Sigma = \{a_1, a_2, \dots a_k\}$ and A be an array over Σ of size m × n. Then the Generalized Parikh Vector of the array A is

$$p(A) = p(u_1) + \frac{1}{2^{|u_1|}} p(u_2) + \Lambda + \frac{1}{2^{|u_1 + u_2 + \Lambda + u_{m-1}|}} p(u_m)$$

where u_i is the ith row of the array A.

Example 3.1. Let $A = \begin{array}{ccc} b & b & a \\ a & b & a \\ b & a & b \end{array}$.

Then $p(A) = p(u_1) + \frac{1}{2^{|u_1|}} p(u_2) + \frac{1}{2^{|u_1 + u_2|}} p(u_3)$ where u_1 = bba, u_2 = aba, u_3 = bab

$$p(u_1) = \left(\frac{1}{2^3}, \frac{1}{2} + \frac{1}{2^2} \right), \quad p(u_2) = \left(\frac{1}{2} + \frac{1}{2^3}, \frac{1}{2^2} \right), \quad p(u_3) = \left(\frac{1}{2^2}, \frac{1}{2} + \frac{1}{2^3} \right)$$

Therefore

$$p(A) = \left(\frac{1}{2^3}, \frac{1}{2} + \frac{1}{2^2}\right) + \frac{1}{2^3}\left(\frac{1}{2} + \frac{1}{2^3}, \frac{1}{2^2}\right) + \frac{1}{2^6}\left(\frac{1}{2^2}, \frac{1}{2} + \frac{1}{2^3}\right)$$

$$= \left(\frac{1}{2^3} + \frac{1}{2^4} + \frac{1}{2^6}, \frac{1}{2} + \frac{1}{2^2} + \frac{1}{2^5} + \frac{1}{2^7} + \frac{1}{2^9}\right)$$

We now introduce the GPV of a partial array

Definition 3.2. Let U be a partial array over $\Sigma = \{a_1, a_2, \ldots a_k\}$ of order m × n. Then the GPV of U, denoted by $p_\Diamond(U)$ is defined as

$$p_\Diamond(U) = p(u_1) + \frac{1}{2^{|u_1|}} p(u_2) + \Lambda + \frac{1}{2^{|u_1 + u_2 + \Lambda + u_{m-1}|}} p(u_m)$$

where $p(u_i)$ is the GPV of the ith row of U.

Example 3.2. Let U be the partial array,

b ◊ a
a b b .
◊ a ◊

Then $p(U) = p(u_1) + \frac{1}{2^{|u_1|}} p(u_2) + \frac{1}{2^{|u_1 + u_2|}} p(u_3)$,

where $u_1 = b\Diamond a$, $u_2 = abb$, $u_3 = \Diamond a\Diamond$

and $p(u_1) = \left(\frac{1}{2^3}, \frac{1}{2}\right)$, $p(u_2) = \left(\frac{1}{2}, \frac{1}{2^2} + \frac{1}{2^3}\right)$, $p(u_3) = \left(\frac{1}{2^2}, 0\right)$

Therefore

$$p(U) = \left(\frac{1}{2^3} + \frac{1}{2^4} + \frac{1}{2^8}, \frac{1}{2} + \frac{1}{2^5} + \frac{1}{2^6}\right)$$

$$= \left(\frac{49}{256}, \frac{35}{64}\right)$$

We define GPV of special arrays such as triangular arrays and polygonal arrays as an special case of rectangular partial arrays.

Definition 3.3. A triangular arrangement of $\dfrac{n(n+1)}{2}$ elements in n rows and n columns, the ith row having i elements, is called a triangular array of size n n. For a given finite alphabet , a triangular array of size m, m $\in$ N can be expressed as a rectangular partial array over Σ of size m $\times$ (2m−1).

The GPV of a triangular array is the GPV of the corresponding rectangular partial array.

Example 3.3.   Consider the triangular array $T = \begin{matrix} a & & \\ a & b & \\ a & a & b \end{matrix}$ of size 3 × 3.

We express T as a partial array as follows:

$$T = \begin{matrix} \Diamond & \Diamond & a & \Diamond & \Diamond \\ \Diamond & a & \Diamond & b & \Diamond \\ a & \Diamond & a & \Diamond & b \end{matrix}$$. Now T is a partial array of size 3 × 5.

We now study polygonal arrays and their Generalized Parikh vectors.

Definition 3.4. A two-dimensional array is a polygonal array if it satisfies one of the following conditions.

(i)   For n ≥ 2, each nth row contains equal or lesser number of entries than (n−1)th row.

(ii)   For n ≥ 2, each nth row contains equal or more number of entries than (n−1)th row.

Example 3.4.   Consider polygonal arrays over a single letter alphabet $\Sigma = \{a\}$.

$$\begin{matrix} a & & & \\ a & & & \\ a & a & & \\ a & a & a & \\ a & a & a & a \end{matrix} \quad \text{and} \quad \begin{matrix} a & a & a \\ a & a & a \\ a & a & \\ a & a & \\ a & & \end{matrix} \quad$$ are special types of polygonal arrays.

A few other polygonal arrays are

$$
\begin{array}{l}
a \\
a \\
a \\
a \\
a\ a\ a\ a
\end{array}
\quad , \quad
\begin{array}{l}
\quad\quad a \\
a\ a\ a \\
a\ a\ a\ a\ a \\
a\ a\ a,\ a\ a\ a \\
a\ a\ a\ a\ a\ a
\end{array}
\quad \text{and} \quad
\begin{array}{l}
\quad\quad\quad a \\
\quad\quad a\ a \\
a\ a\ a \\
a\ a\ a
\end{array}
\text{ called}
$$

as L shaped, % shaped, left Δ and right Δ arrays respectively. Interestingly, all these polygonal arrays form a particular shape and to find its GPV, we treat them as partial arrays and apply Definition 3.2 to them.

Given the GPV of a partial array, it is possible to recognize the type of polygonal array. This is given in the following propositions.

Proposition 3.1. A rectangular partial array T of size m × m over Σ such that $|\Sigma| = $ k with GPV of T, $p(T) = (p_1, p_2, \ldots, p_k)$ Σ represents

   (i) a left triangle array if the GPV of T satisfies the following condition:

$$p_1 + p_2 + \cdots + p_k =$$

$$\frac{1}{2} + \left(\frac{1}{2^{m+1}} + \frac{1}{2^{m+2}} \right) + \left(\frac{1}{2^{2m+1}} + \frac{1}{2^{2m+2}} + \frac{1}{2^{2m+3}} \right) + \left(\frac{1}{2^{3m+1}} + \Lambda\ 4\ \text{terms} \right) + \Lambda$$

(ii)   a right triangle array of size m × m, if the GPV of T satisfies the condition:

$$p_1 + p_2 + \Lambda + p_k = \frac{1}{2^m} + \left(\frac{1}{2^{2m}} + \frac{1}{2^{2m-1}} \right) + \left(\frac{1}{2^{3m}} + \frac{1}{2^{3m-1}} + \frac{1}{2^{3m-2}} \right)$$

$$+ \Lambda + \left(\frac{1}{2^{m^2}} + \frac{1}{2^{m^2-1}} + \Lambda + \frac{1}{2^{m^2-m+1}} \right)$$

Proof: We consider a left triangle array of size m × m as given in the theorem. This array is of the form

$$
m \left\{
\begin{array}{l}
a_i \\
a_i\ a_i \\
a_i\ a_i\ a_i \\
\quad M \\
\underbrace{a_i\ a_i\ \Lambda\ a_i}_{m}
\end{array}
\right.
\qquad \text{where each } a_i \in \Sigma, i \in \{1, 2, \ldots, k\}
$$

This can be represented as a rectangular partial array T of size $m \times m$ as follows:

$$m \begin{cases} a_i & \Diamond & \Diamond & \Diamond \\ a_i & a_i & \Diamond & \Diamond \\ a_i & a_i & a_i & \Diamond \\ & M & \Diamond & \Diamond & \Diamond \\ a_{i1} & a_{i2} & \Lambda & a_{i3} \end{cases}$$

Applying definition 3.2, we find that

$$p_1 + p_2 + \cdots + p_k = \left(\frac{1}{2} + \frac{1}{2^{m+1}} + \frac{1}{2^{m+2}} + \frac{1}{2^{2m+1}} + \frac{1}{2^{2m+2}} + \frac{1}{2^{2m+3}} + \frac{1}{2^{3m+1}} + \Lambda \ 4 \ \text{terms} + \Lambda \right)$$

A similar argument holds for a right triangle array and (ii) can be proved.

Proposition 3.2. The Generalized Parikh vector of a partial array B of size n m, over Σ such that $|\Sigma| = k$, represents that of a L shaped polygonal array over the same , if the following condition is satisfied.

If $p(B) = (p_1, p_2, \ldots, p_k)$ is the GPV of B, then

$$p_1 + p_2 + \Lambda + p_k = \frac{1}{2} + \frac{1}{2^{m+1}} + \frac{1}{2^{2m+1}} + \Lambda \ \frac{1}{2^{nm-m+1}} + \frac{1}{2^{nm-m+2}} + \Lambda + \frac{1}{2^{nm}}$$

Proof: An L-shaped array of size $m \times n$ over Σ is of the form

$$m \begin{cases} a_i \\ a_i \\ a_i \\ M \\ a_{i1} \ a_{i2} \ \Lambda \ a_{i3} \end{cases} \quad \text{where each } a_i \in \Sigma, i \in \{1, 2, \ldots, k\}.$$

This can be represented by a rectangular partial array B of size $m \times n$ as follows:

$$m \begin{cases} a_i & \Diamond & \Diamond & \Diamond \\ a_i & \Diamond & \Diamond & \Diamond \\ a_i & \Diamond & \Diamond & \Diamond \\ & M & \Diamond & \Diamond & \Diamond \\ a_{i1} & a_{i2} & \Lambda & a_{i3} \end{cases} .$$

Applying definition 3.2 to the array B, we have

$$p_1 + p_2 + \Lambda + p_k = \frac{1}{2} + \frac{1}{2^n}\left(\frac{1}{2}\right) + \frac{1}{2^{2n}}\left(\frac{1}{2}\right) + \Lambda \ \frac{1}{2^{(n-1)m}}\left(\frac{1}{2} + \frac{1}{2^2} + \Lambda + \frac{1}{2^m}\right)$$

$$= \frac{1}{2} + \frac{1}{2^{n+1}} + \frac{1}{2^{2n+1}} + \Lambda \ \frac{1}{2^{nm-n+1}} + \frac{1}{2^{nm-n+2}} + \Lambda + \frac{1}{2^{nm}}$$

4. Operators on Generalized Parikh Vectors

In this section we have defined a few operators on GPV.

Definition 4.1. For two words w_1, $w_2 \in \Sigma^+$, the GPV of the catenated word $w_1 \% w_2$ is defined as

$p(w_1 \% w_2) = p(w_1) + \frac{1}{2^{|w_1|}} p(w_2)$. This operator "%" known as the catenation operator, operates

on the GPVs of two words to yield the GPV of the catenated word.

Example 4.1. Let $w_1 = $ aaba and $w_2 = $ bbab

$$p(w_1) = \left(\frac{1}{2} + \frac{1}{2^2} + \frac{1}{2^4}, \frac{1}{2^3}\right), \ p(w_2) = \left(\frac{1}{2^3}, \frac{1}{2} + \frac{1}{2^2} + \frac{1}{2^4}\right)$$

$$p(w_1 \mathrm{o} w_2) = \left(\frac{1}{2} + \frac{1}{2^2} + \frac{1}{2^4}, \frac{1}{2^3}\right) + \frac{1}{2^4}\left(\frac{1}{2^3}, \frac{1}{2} + \frac{1}{2^2} + \frac{1}{2^4}\right)$$

$$= \left(\frac{1}{2} + \frac{1}{2^2} + \frac{1}{2^4} + \frac{1}{2^7}, \frac{1}{2^3} + \frac{1}{2^5} + \frac{1}{2^6} + \frac{1}{2^8}\right)$$

Definition 4.2. For a word w over $\Sigma = \{a, b, c\}$ of length n, the GPV of w, namely $p(w) = (p_1, p_2, p_3)$. The right shift operator S_R of the GPV of w denoted as

$S_R[p(w)] = S_R[(p_1, p_2, p_3)]$ is $S_R\left[\frac{1}{2^i}\right] = \frac{1}{2^{i-1}}$ for $i = 1$ to n and $S_R\left[\frac{1}{2^0}\right] = \frac{1}{2^n}$

Definition 4.3. The left shift operator S_L of the GPV of the word w of length n, over

$\Sigma = \{a, b, c\}$ denoted by $S_L[p(w)] = S_L[(p_1, p_2, p_3)]$ is defined as $S_L\left[\frac{1}{2^i}\right] = \frac{1}{2^{i+1}}$ for

$i = 1$ to n and $S_L\left[\frac{1}{2^{n+1}}\right] = \frac{1}{2}$ where $p(w) = (p_1, p_2, p_3)$ is the GPV of the word w.

Definition 4.4. Let x and y be two words over Σ; x is said to be equivalent to y, if and only if $x = uv$, $y = vu$ for $u, v \in \Sigma^*$.

Example 4.2. Let w = bacab. $p(w) = \left(\dfrac{1}{2^2} + \dfrac{1}{2^4}, \dfrac{1}{2} + \dfrac{1}{2^5}, \dfrac{1}{2^3} \right)$

Then $S_L(p(w)) = S_L\left(\left(\dfrac{1}{2^2} + \dfrac{1}{2^4} \right), \left(\dfrac{1}{2} + \dfrac{1}{2^5} \right), \dfrac{1}{2^3} \right) = \left(\dfrac{1}{2^3} + \dfrac{1}{2^5}, \dfrac{1}{2^2} + \dfrac{1}{2}, \dfrac{1}{2^4} \right)$

The operators right shift and left shift, operates on the GPV of a word w to yield the GPV of another word equivalent to w.

Definition 4.5. The reversal operator on the GPV of a word, denoted by R[p(w)] is defined as

$R\left[\dfrac{1}{2^i} \right] = \dfrac{1}{2^{n-i+1}}$, for i = 1, 2, …, n where n is the length of the word w.

We recall the definition of circular strings and circular languages [3,4]

Let " be a finite alphabet. Define an equivalence relation " ~ " on " such that x ~ y if and only if x= uv ; y = vu for $u, v \in \Sigma^*$. For every linear string $x \in \Sigma^*$, we can associate a circular string denoted by — x, by defining it as an equivalence class of strings under the relation "~". We denote the set of all circular strings over Σ by Σ—

Example 4.3 A circular string ^aabbcc is shown in Figure below.
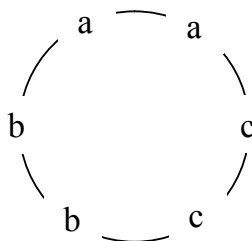
We consider palindromes and characterize their GPV in the following proposition.

Proposition 4.1. Given two words w_1 and w_2 of length n, with GPVs $p(w_1) = (a_1, a_2, a_3)$, $p(w_2) = (b_1, b_2, b_3)$ and their Parikh vectors being $\pi(w_1) = (p_1, p_2, p_3)$, $\pi(w_2) = (q_1, q_2, q_3)$. If w_1 and w_2 are two different linearizations of the same circular word then

(i) $a_1 + a_2 + a_3 = b_1 + b_2 + b_3$

(ii) $p_1 = q_1, p_2 = q_2$ and $p_3 = q_3$

(iii)   Each a_j and b_j, j = 1, 2, 3 are of the form   with i = 1 to n, such that the number of

terms in $a_j = p_j$ and number of terms in each $b_j = q_j$.

Proof: Condition (i) ensures that w_1 and w_2 are of the same length. Condition (ii) ensures that the number of letters in Σ in both w_1 and w_2 are the same. Condition (iii) say that each a_j and b_j, j = 1, 2, 3 are of the form with i = 1 to n, such that the number of terms in $a_j = p_j$ and number of terms in each $b_j = q_j$.

Theorem 4.1. If $\wedge x$ is a circular string of length n then (n−1) linearizations of $\wedge x$ can be obtained by recursively applying the right shift operator (left shift operator) to the GPV of any one of its linearized form.

Proof: Let $\wedge x$ be a given circular word. Let aw be one of its linearized forms where a is made to occur in the first position. There are (n−1) ways of writing x by shifting a right side once. Any two of the linearized words of x satisfy the three conditions of proposition 4.1.

This is seen in the following example. $\sum \dfrac{1}{2^i}$

$\wedge cabab = $

$$\begin{matrix} & & c & & \\ & a & & b & \\ & & b & a & \end{matrix}$$

$$p(cabab) = \left(\frac{1}{2^2} + \frac{1}{2^4} , \frac{1}{2^3} + \frac{1}{2^5} , \frac{1}{2} \right)$$

$$S_R[p(cabab)] = \left(\frac{1}{2} + \frac{1}{2^3} , \frac{1}{2^2} + \frac{1}{2^4} , \frac{1}{2^5} \right) = p(ababc)$$

Similarly the other linearizations of $\wedge cabab$ can be obtained by using right shift operator.

Proposition 4.2. Any nonempty binary word $w \in \Sigma^+$ be a palindrome. If its GPV $p(w) = (p_1, p_2)$ then it satisfies the following.

(i)   If $|w| = 2n$, then each p_i (i = 1, 2) is the finite series of even number of terms and can be expressed as a sum of terms of the form and for some j, $j \in \{0, 1, …, n−1\}$.

(ii) If $|w| = 2n+1$, then p_i $(i = 1, 2)$ is the finite series of even number of terms for $i = 1$ or 2, but not both, and can be expressed as a sum of terms of the form and for some j, j $\in$ {0, 1, …, n−1} and is in the series of odd number of terms.

Proof: From the definition of the palindrome and GPV of a word it is easy to verify the conditions (i) and (ii) of the theorem.

5. Conclusion

In this paper the concept of Generalized Parikh vectors for words have been extended to arrays and partial arrays. Further, some properties of special types of arrays have been given and operators on GPV have been defined and studied.

References

1. Jansirani N. and Dare V.R., Studies on Combinatorial properties of infinite arrays, Ph.D. Thesis, (2014).

2. Lothaire M., Combinatorics on words, Addison-Wesley, (1983).

3. Parikh R.J., On the context-free languages, Journal of the Association for Computing Machinery, 13 (1966), 570-581.

4. Robinson T., A Study on circular languages, patterns and map systems, Ph.D. Thesis, October 1999.

5. Rosenfeld A., A note on cycle grammars, Information control 27 (1975), 374-377.

6. Siromoney R. and Dare V.R., On Infinite Words obtained by selective substitution grammars, Theoretical Computer Science, 39 (1985), 281-295.

SURVEY ON WIRELESS SENSOR NETWORK

*N.Aravinthan, **K. Geetha

Abstract

A wireless sensor network is an emerging technique nowadays. This Wireless Sensor Network (WSN) is used in military applications for monitoring the area, industrial application to monitor the machine and to make control over it, in mobile multimedia to track audio and video etc. Based on the application, the deployment is different. Research on WSN faces different issues since it has to communicate directly with a centralized controller or satellite. In this, paper we discuss about various types of wireless sensor networks in terms of cost and issues in the maintenance of WSN, techniques used for localization and synchronization and the area covered by the networks.

Keywords

Wireless Sensor Networks, Localization, Synchronization, Unstructured WSN, Structured WSN.

1. Introduction

Recent developments in wireless communications have enabled the communication services with low-cost, low-power and multi functional. Wireless sensor networks consist of the number of sensor nodes widely distributed, communicate data to a main location, monitor physical or environmental conditions such as temperature, sound, climate, etc. They are also useful in detection of foreign chemical agents in the air and the water, enable pervasive computing environment in hospitals to monitor the conditions of patients etc. The sensor nodes perceive the data, process them, and communicate to the WSN components. The more modern networks support of sending data in bidirectional and also enable the control of sensor equipments. The WSN is built from hundreds to thousand nodes and each node is connected to one or more sensors.

Some sensors perform only sensing data and they are small in size with limited processing

*Research Scholar, Department of Computer Science, Bharathiar University- Coimbatore 641 046

**Assistant Professor, Department of Computer Science, Bharathiar University- Coimbatore 641 046

and computing resources. The positions of the sensors are to be carefully engineered so as to enable better communications among them. These sensors are inexpensive compared to traditional sensors. Each sensor network node has several parts. A radio transceiver with an internal antenna or external antenna for connection, a micro controller, an electronic circuit for interfacing with the sensors and an energy source[1]. They transmit time series of the sensed phenomenon to the central nodes where computations are performed and the data are fused.

Sensor nodes perceive information from the environment, based on some local decision process, then they are transmitted to the user. It is difficult to locate the location of the sensors which have limited memory and deployed in various locations, a radio is used in wireless communication to transfer the data to a base station. In most cases of sensor nodes, battery is the main power source.

The WSN topology is different from a simple network to advanced network. Simple networks can be interconnected with few sensor nodes in a simple interconnection structure like star network. If more number of nodes deployed densely, the neighbor nodes will be very close in which multi hop wireless network can be employed. So, the design of the WSN varies based on the application.
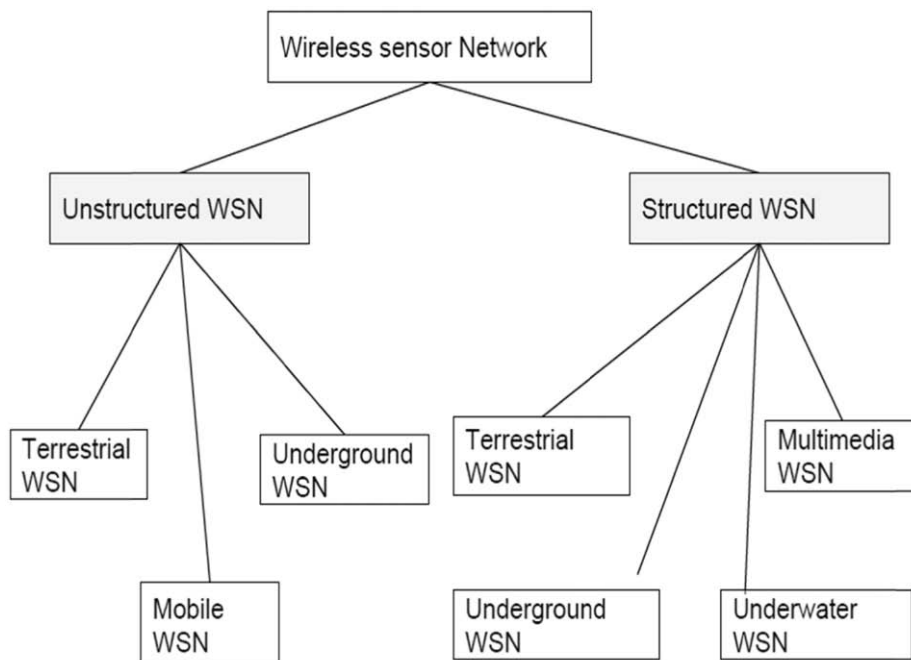

Figure 2.1. Classification of Wireless Sensor Networks

2. Classification of Wireless Sensor Networks

WSN Mainly classified into two types: structured and unstructured. Based on the installation of sensors and area which was covered by the network it can be classified into terrestrial, underground, underwater, multimedia and mobile WSN as shown in fig. 2.1. Cost and issues related to the WSN are tabulated in Table 1.

In a structured WSN, sensor nodes are deployed in a pre-planned manner. So, the location or the selection of the node as a base station is set/known prior. The advantage of a structured

Table 1. Cost and Challenges of Various Wireless Sensor Networks

Type of WSN	Cost	Challenges
Terrestrial WSN	Low	Maintaining network connectivity
Underground WSN	Moderate	Handling Signal loss Battery replacement or recharging.
Underwater WSN	High	Limited bandwidth, Long propagation delay Signal fading issue. Failure due to environmental Conditions. Battery replacement or recharging.
Multimedia WSN	Moderate	High bandwidth demand, High energy consumption, Quality of service (QoS) provisioning, Data processing and compressing techniques, Cross-layer design
Mobile WSN	Moderate	Deployment, Localization, Self-organization, Navigation and control, Area coverage, Energy management, Maintenance, Processing data

network is that it can be deployed with fewer nodes with simple network structures, so as to reduce maintenance cost and to deduct the failure nodes easily[1].

In unstructured WSN, sensor nodes are deployed in an adhoc manner which leads the unbounded coverage area. So, in this type of WSN, the structure of the network cannot be planned. Some of the issues in unstructured WSN are network maintenance such as managing connectivity, detecting failures, etc.

2.1 Terrestrial WSN

Terrestrial WSN is implemented by hundreds to thousands of Wireless sensor nodes in a given area under adhoc i.e. Unstructured or structured manner. In unstructured implementation, sensor nodes can be dropped from a plane and randomly placed in an area where we want to have the sensors. In the structured implementation, grid placement, optical placement, 2D and 3D dimensional placement models can be used. Terrestrial sensor nodes must able to communicate with the base station to transfer the data. One disadvantage in type of network is the maintenance of the battery power which cannot be recharged easily. One alternate solution for this problem is the use of secondary power sources such as solar cells. Sensor nodes have to save energy and this can be achieved in terrestrial WSN, with multi hop optimal routing[1].

2.2 Under Water WSN

In underwater WSN, number of sensor nodes are set under the water area in specific distances. Autonomous underwater vehicles are used for searching or gathering data from the sensor nodes. The underwater wireless communications are established through acoustic waves.Underwater sensor nodes must be able to self configure and correct to the rugged ocean environment. Underwater sensor nodes are provided with a limited battery which cannot be easily replaced or rechargeable. The energy saving for underwater wireless sensor nodes involves developing efficient underwater communication and networking techniques[2][3][4].

2.3 Underground WSN

The underground wireless sensor network consists of sensor nodes, which are set in underground, cave or mine to monitor underground conditions. Additional sink nodes are located above ground to transmit information from the sensor nodes to the base station. Compare with terrestrial WSN the implementation of an underground WSN requires careful planning and energy, cost considerations. Energy is the most important concern in underground WSN. Once sensors are set under the ground, it is difficult to recharge or replace the battery. To increase the lifetime of the network, well organized communication protocols are proposed[5][6][7][8].

2.4 Multimedia WSN

It is used to monitor and track the events in the form of multimedia such as video, audio and imaging. Multimedia WSN consist of low cost sensor nodes equipped with cameras and microphones. These sensor nodes are interconnected with each other over a wireless connection for data retrieval, process, correlation and compression.Transmission with high bandwidth in Multimedia WSN is required for the better results. High data rate leads to high energy consumption.In this type of network,the performance can be significantly improved by undergoing the filter process, compression and merging contents[9][10].

2.5 Mobile WSN

Mobile WSN consist of collection of sensor nodes, which can move on their own and interact with the physical environment. Mobile nodes have the ability to sense, compute and communicate like static nodes. Mobile nodes have the ability to reposition and organize themselves in the network. A mobile WSN can start off with some initial deployment and nodes can then spread out to gather information. Information gathered by a mobile node can be communicated to another mobile when only they are within range of each other. Another difference is data distribution. In a static WSN, data can be distributed using fixed routing or flooding, while dynamic routing is used in a mobile WSN[2].

3. Network Services

3.1 Localization

In the wireless sensor network, sensor nodes are deployed in the environment in a structured manner, which means the sensor nodes don't have a prior knowledge of their own location. In other words, localization is to determine the location of the node. There are several localization techniques found in the literature and some of them are presented here.

Anchor Based Localization Scheme: In this technique, the position of few nodes is known. These nodes are known as anchor nodes. With the help of these anchor nodes the location of other un-localized nodes are determined. The accuracy of location,highly depends on the number of anchor nodes. It has the problem due to environmental conditions and it is not used in large networks. e.g. Global Positioning System(GPS).

Anchor Free Localization Scheme: There is no anchor node available. So instead of calculating absolute positions of the nodes, algorithms calculate the relative positions of the nodes[11][12].Some of the techniques or algorithms for WSN found in the literature are presented in Table 2.

Table 2. Localization Techniques/Algorithms

Technique/Algorithm	Description
Moore's algorithm	Location estimation without the use of GPS (or) Fixed beacon nodes[13].
Radio Interferometric Positioning System	Two radio transmitters are placed at different locations and set at slightly different radio frequencies to provide ranging information for localization. At least two receivers are needed to calculate the phase offset of the observed signals[14].
Spotlight	The main idea of the Spotlight localization system is to generate controlled events in the field where the sensor nodes are deployed[13].
Secure localization	Secure localization focuses on securing the localization process. The goal is to prevent malicious beacon nodes from providing false location of the sensors. Sensors rely on beacon information to compute their position[15].
Mobile-assisted localization (MAL)	Mobile-Assisted Localization (MAL) utilizes a mobile user (a human or robot) to assist in collecting distance information between itself and static sensor nodes for node localization. The goal is to re-construct the position of the nodes given a graph with measured distance edges[16].
Weighted centroid method	The position of the target device is calculated by the known positions of the anchor nodes in the transmission range. Although this algorithm is very simple, efficient, easy to implement and needs low computational operations, it produces a lower level of precision[16].
Point in Triangle method	The Point in Triangle method is a range-free localization scheme. In this approach the target device sends a beacon message that is received by the fix nodes[16].

Technique/Algorithm	Description
Centralized localization	Centralized localization techniques involve data transfer to a central node in order to compute the location for each node. Communication with centralized computing is expensive, and sending data serially by time within the network introduces latency[17].
Decentralized or distributed localization	Decentralized or distributed localization techniques depend on each sensor node being able to determine its location. It is only performed within the limited communication with nearby nodes. Distributed localization techniques do not require centralized computation[17].

3.2 Synchronization

The synchronization in WSN mainly deals with time synchronization and calibration. Lack in time synchronization leads to the problem in both routing and power saving of sensor nodes, which results in reduction of the lifetime of the network. One of the time synchronization method is global time synchronization, it allows the nodes to cooperate and transmit the data in a particular scheduled manner. The energy is saved when there is no collision between the nodes and also no retransmission[18]. Techniques used for synchronization are presented in the Table 3.

3.3 Coverage

Coverage problem is also an important and fundamental issue in sensor networks, which reflects how well a sensor network is monitored or tracked by sensors. In literature, sensor activation, scheduling under constraints on the covering of targets is defined as coverage problem. There are three types of coverage : Area, Point(target) and Path[25].

3.3.1 Area Coverage problem

In this type, there will be a set of sensors distributed over a geographical region to monitor a specified area. The problem is to find the minimum number of active sensors such that every physical point in the area is monitored by at least a working sensor. There exists various forms of area coverage problems: k-coverage, m-connected, k-coverage m-connected problems.

3.3.2 Point coverage:

Generally point coverage is a special case of area coverage problem, in which a set of sensors is given and distributed over a geographical region to monitor a set of points. The objective

Table 3. Synchronization Techniques/Algorithms

Technique/ Algorithm	Description
Uncertainty-driven approach	This approach uses long-term empirical measurements to evaluate and analyze three key parameters that influence long-term synchronization. The parameters are synchronizing rate, history of past synchronization beacons, and the estimation scheme[19].
Lucarelli's algorithm	Synchronization with bidirectional nearest neighbor coupling[20].
Reachback firefly algorithm	The algorithm is based on a mathematical model explaining how neurons and fireflies spontaneously synchronize. The firefly synchronization is robust and adapts to changes such as losses, adding nodes, and link changes[21].
Timing-sync protocol for sensor network (TPSN)	TPSN provides time synchronization for every sensor node in the network. TPSN is based on a conventional sender–receiver synchronization approach. TPSN has two phases, a level discovery phase and synchronization phase[20].
Clock-sampling mutual network synchronization (CSMNS)	CSMNS is a distributed and autonomous network synchronization approach. CSMNS does not depend on a centralized node to synchronize time nor does it depend on special circuitry to send continuous pulses. It is a non-hierarchical approach that supports single and multi-hop communication[21].
Time synchronization (TSync)	TSync is an accurate, lightweight, flexible, and comprehensive in finding time solution for WSNs. TSync uses multi-channel radios for frequency diversity to reduce packet collisions and interferences[22].
Global synchronization	All-node-based method, cluster-based method, and fully localized diffusion based method. The all-node-based method routes a message along a specified cycle path and synchronize all the nodes along the path. In the cluster-based method, the network is synchronized using a hierarchical approach. The fully localized diffusion-based method achieves global synchronization by averaging all clock readings and adjusting each clock in the network to the average time[23].

Technique/ Algorithm	Description
Synchronization protocol classification	Synchronization protocols based on two kinds of features: application-dependent features and synchronization issues. Application dependent features are classified into single-hop vs multi-hop networks, stationary vs mobile networks, and MAC layer-based vs standard-based approach. The Synchronization issue involves sensors adjusting their local clocks to a common time scale[24].

of point coverage problem is to cover a set of point (target) with known location that need to be monitored. It focuses on the determination on the exact location of the sensor nodes. It is also implemented in area coverage where some points remain undetected due to some problems.

Path coverage is deployed in WSN to get the specific path and report about the efforts made by the intruders if any. Based on the application, sensors can be deployed specifically or randomly. Due to the randomness of the sensor location, network coverage expresses a stochastic behavior and the desired (full) path coverage is not guaranteed[26].

4.Conclusion

Wireless Sensor networks have a wide area of applications which includes machine monitoring, surveillance systems, tracking systems, etc. Every application covers different features and requirements. In the future, development of new communications protocols & algorithm design are needed. In this paper, the classification of WSN, some of the techniques used in localization, synchronization and area covered by the WSN are reviewed.

References

1. I.F. Akyildiz, W. Su, Y. Sankara Subramaniam, E. Cayirci, "A Survey On Sensor Networks", IEEE Communications Magazine 40 (8) (2002) 104–112.

2. M.Stojanovic, "Acoustic (underwater) communications in Encyclopedia of Telecommunications", J. G. Proakis, Ed. John Wiley and Sons, 2003.

3. J. Proakis, J. Rice, E. Sozer, and M. Stojanovic, "Shallow Water Acoustic Networks In Encyclopedia Of Telecommunications", J. G. Proakis, Ed. John Wiley and Sons, 2003.

4. L. Freitag and M. Stojanovic, "Acoustic Communications For Regional Undersea Observatories," in Proceedings of Oceanology International, London, U.K., mar 2002.

5. R. Musaloiu, A. Terzis, K. Szlavecz, A. Szalay, J. Cogan, J.Gray," Life Under Your Feet: A Wireless Soil Ecology Sensor Network", in: EmNetS'06: Proceedings of the Third IEEE Conference on embedded networked sensors, 2006.

6. R. Cardell-Oliver, K. Smettem, M. Kranz, K. Mayer, "A Reactive Soil Moisture Sensor Network Design And Field Evaluation", International Journal of Distributed Sensor Networks 1 (2) (2005) 149–162.

7. I.F. Akyildiz, E.P. Stuntebeck, "Wireless Underground Sensor Networks: Research Challenges", Ad-Hoc Networks 4 (2006) 669–686.

8. J. Heidemann, Y. Li, A. Syed, J. Wills, W. Ye, "Underwater Sensor Networking: Research Challenges And Potential Applications", in: Proceedings of the Technical Report ISI-TR-2005-603, USC/Information Sciences Institute, 2005.

9. E. Gurses, O.B. Akan, "Multimedia Communication In Wireless Sensor Networks", Ann. Telecommun. 60 (7–8) (2005) 799–827.

10. S. Misra, M. Reisslein, G. Xue, "A Survey of Multimedia Streaming In Wireless Sensor Networks",.

11. He, T., Huang, C., Blum, B.M., Stankovic, J.A., Abdelzaher, "T.: Range-free Localization Schemes for Large Scale Sensor Networks", In: MobiCom '03: Proceedings of the 9th Annual International Conference on Mobile Computing and Networking, pp. 81–95. ACM, New York, 2003.

12. Attila K. Varga ," Localization Techniques In Wireless Sensor Networks", Production Systems and Information Engineering Volume 6 (2013), pp. 81-90

13. D. Moore, J. Leonard, D. Rus, S. Teller," Robust Distributed Network Localization With Noisy Range Measurements", in: Proceedings of the Sensys'04, San Diego, CA, 2004.

14. Q. Fang, J. Gao and L. J. Guibas, "Locating And Bypassing Routing Holes In Sensor Networks," in Proceedings Of Ieee Infocom, 2004.

15. L. Lazos, R. Poovendran, SeRLoc: "'Secure Range Independent Localization For Wireless Sensor Networks", in: First IEEE International Conference on Mobile Ad hoc and Sensor Systems, Fort Lauderdale, FL, 2004.

16. R. Stoleru, T. He, J.A. Stankovic, D. Luebke, "A High-Accuracy, Low-Cost Localization System For Wireless Sensor Networks", in: Proceedings of the Third International Conference on Embedded Networked Sensor Systems (Sensys), San Diego, CA, 2005.

17. R. Manzoor, "Energy Efficient Localization In Wireless Sensor Networks Using Noisy Measurements", [M.S. thesis], 2010.

18. M. Maroti, B. Kusy, G. Simon, A. Ledeczi, "Synchronization of Pulse Coupled Biological Oscillators", SIAM 50 (1990) 1645–1662.

19. Ganeriwal, Saurabh, et al. ,"Estimating Clock Uncertainty For Efficient Duty-Cycling In Sensor Networks" ,IEEE/ACM Transactions on Networking (TON)17.3 (2009): 843-856.

20. Lucarelli, Dennis, and I-Jeng Wang, "Decentralized Synchronization Protocols With Nearest Neighbor

Communication", Proceedings of the 2nd international conference on Embedded networked sensor systems. ACM, 2004.

21. Rentel, Carlos H., and Thomas Kunz.,"A Clock-Sampling Mutual Network Time-Synchronization Algorithm For Wireless Ad Hoc Networks" ,IEEE Wireless Communications and Networking Conference, 2005. Vol. 1. IEEE, 2005.

22. Dai, Hui, and Richard Han,"Tsync: A Lightweight Bidirectional Time Synchronization Service For Wireless Sensor Networks", ACM SIGMOBILE Mobile Computing and Communications Review 8.1 (2004): 125-139.

23. Li, Qun, and Daniela Rus,"Global Clock Synchronization In Sensor Networks", IEEE Transactions on computers 55.2 (2006): 214-226.

24. Sundararaman, Bharath, Ugo Buy, and Ajay D. Kshemkalyani,"Clock Synchronization For Wireless Sensor Networks: A Survey", Ad hoc networks 3.3 (2005): 281-323.

25. Jie Chen and XenofonKoutsoukos, "Survey On Coverage Problems In Wireless Ad Hoc Sensor Networks", IEEE SouthEastCon 2007. Richmond, VA, March 22-25, 2007.

26. M.X. Cheng, L. Ruan, and Weili Wu, "Achieving Minimum Coveragebreach Under Bandwidth Constraints In Wireless Sensor Networks", Infocom'05.

TWO DIMENSIONAL BOUNDARY LAYER SLIP FLOW OF CASSON FLUID OVER A STRETCHING SHEET WITH ALIGNED MAGNETIC FIELD AND MASS FLUX

*Dr. S. Anuradha and *M.Priya

Abstract

The present study explores two dimensional boundary layer slip flow of Casson fluid over a stretching sheet with aligned magnetic field and mass flux. A mathematical formulation has designed for velocity, momentum, temperature and concentration profiles. The governing partial differential equations are reduced to a system of ordinary differential equations using similarity transformation and then solved numerically with Runge–Kutta sixth order iteration scheme. The numerical results of the flow characteristics are presented graphically.

Keywords

Casson fluid, Magnetohydrodynamics (MHD), Angle parameter(γ), Casson parameter(â), Slip parameter(L), Magnetic parameter(Mn), Lewis number (Le), Prandtl number(Pr), Nusselt number(Nu), Sherwood number(Sh).

1. Introduction

Casson fluid model is a non-newtonian fluid. In 1995 Casson fluid model was introduced by Casson. This model is based on a two-phase suspension. It can be defined as a shear thinning liquid and assumed to have an infinite viscosity at zero rate of shear, a yield stress below which no flow occurs and a zero viscosity at an infinite rate of shear .The best examples are jelly, soup, honey, tomato sauce etc. The theory of Casson fluid flow over a stretching sheet has become several applications in technology and industry. The various applications are dye, wire drawing, glass blowing, paper production, hot rolling, food stuffs and many others.

* Professor & Head in Department of Mathematics, Hindusthan College of Arts & Science, Coimbatore-641028, Tamilnadu, India, email:anu.prasanthi@gmail.com.

* Research Scholar in Department of mathematics, Hindusthan College of Arts & Science, Coimbatore-641028, Tamilnadu, India, email:priya.jeni28@gmail.com.

In this study, we have observed that magnetic field effect on second order slip flow of nanofluid over a stretching/shrinking sheet with thermal radiation effect investigated by Abdul Hakeem *et al.* [1]. Reddy [2] reported MHD flow of a Casson fluid over an exponentially inclined permeable stretching surface with thermal radiation and chemical reaction. Hayat *et al.* [3] have analyzed soret and dufour effects on MHD flow of Casson fluid. An unsteady MHD mixed convection slip flow of Casson fluid over a non-linearly stretching sheet examined by Imran *et al.* [4]. Pramanik [5] have explained Casson fluid flow and heat transfer past an exponentially porous stretching surface in presence of thermal radiation. Sharada and Bandari [6] have studied MHD mixed convection flow of a Casson fluid over an exponentially stretching surface with the effects of soret, dufour, thermal radiation and chemical reaction. Slip effects on MHD flow of Casson fluid over an exponentially stretching sheet in presence of thermal radiation, heat source/sink and chemical reaction have established by Saidulu and Lakshmi [7]. Effect of chemical reaction on slip flow of MHD Casson fluid over a stretching sheet with heat and mass transfer have investigated by Sathies and Gangadhar [8]. Shehzad *et al.* [9] have studied effects of mass transfer on MHD flow of Casson fluid with chemical reaction and suction. Vijayalaxmi *et al.* [10] have analyzed on slip flow of Casson nanofluid over a nonlinear stretching sheet with chemical reaction in effect of aligned magnetic field.

2. Formulation of the problem

Let us consider the problem of the steady, laminar, two-dimensional boundary layer and an incompressible Slip flow of Casson fluid over a Stretching sheet. Here B_0 is an Aligned magnetic field of strength applied along y-direction. An acute angle $\beta = 90^{\circ}$, at this angle the magnetic field acts like transverse magnetic field ($\sin 90^{\circ} = 1$). The rheological equation of state for an isotropic and incompressible flow of a Casson fluid can be written as

$$\tau_{ij} = \begin{cases} 2(\mu_B + p_y / \sqrt{2\pi})e_{ij}, \pi > \pi_c \\ 2(\mu_B + p_y / \sqrt{2\pi_c})e_{ij}, \pi < \pi_c \end{cases}$$

Where $\pi = e_{ij}$ and e_{ij} denote the $(i, j)^{th}$ component of the deformation rate, π is the product of the component of deformation rate with itself, is the yield stress of the fluid, π_c is a critical value of this product based on the non-Newtonian model and μ_B is plastic dynamic viscosity of the non-Newtonian fluid. Let u and are the velocity components of and directions respectively, the governing boundary layer equations for two dimensional incompressible Casson fluid are given by

$$(1)$$

$$uu_x + vu_y = \vartheta\left(1+\frac{1}{\beta}\right)u_{yy} - \frac{\sigma B_0^2 u}{\rho}\sin^2\gamma \tag{2}$$

$$uT_x + vT_y = \frac{k}{\rho c_p}T_{yy} \tag{3}$$

$$uC_x + vC_y = D_B C_{yy} \tag{4}$$

Here   is the kinematic viscosity,   is the fluid density,   is the Casson fluid parameter

and σ is the electrical conductivity.   is the thermal conductivity, c_p is

the specific heat of constant pressure. D_B is the Brownian diffusion.

The corresponding boundary conditions for the velocity, Temperature and Concentration fields
are

$$u = ax + lu_y, v = v_w \qquad T = T_w = T_\infty + A\left(\frac{x}{l}\right)^2 \qquad \qquad$$

$$C \rightarrow C_\infty \qquad\qquad \text{as} \qquad\qquad (5)$$

Here   is the characteristic length, T_w is the temperature of the sheet and T_∞ is the

temperature of the fluid far away from the sheet. C_w and C_∞ are concentration of the sheet and

the fluid far away from the sheet. We introduce the following similarity transformation

$$u = axf_\eta, v = -\left(a\vartheta\right)^{\frac{1}{2}}f \text{ and } \eta = \left(\frac{a}{\vartheta}\right)^{\frac{1}{2}}y$$

$$\theta(\eta) = \frac{T - T_\infty}{T_w - T_\infty} \qquad \phi(\eta) = \frac{C - C_\infty}{C_w - C_\infty} \tag{6}$$

Using similarity variables (6), continuity equation (1) is trivially satisfied. Equations (2), (3) and
(4) take the non-dimensional form

$$\left(1 + \frac{1}{\beta}\right) f_{\eta\eta\eta} + ff_{\eta\eta} - f_{\eta}^2 - Mnf_{\eta} \sin^2 \gamma = 0 \tag{7}$$

$$\theta_{\eta\eta} + \Pr f\theta_{\eta} - 2\Pr f_{\eta}\theta = 0 \tag{8}$$

$$\phi_{\eta\eta} + Lef\phi_{\eta} - Lef_{\eta}\phi = 0 \tag{9}$$

With corresponding boundary conditions

$$\theta(\eta) = 1 \qquad\qquad \text{at}$$

$$\qquad\qquad \text{as} \tag{10}$$

The subscript denotes differentiation with respect to η. Where is the magnetic parameter $(Mn = \frac{\sigma B_0^2}{\rho a})$, L is the slip parameter $(L = l\sqrt{a/\vartheta})$, $\Pr = \frac{\mu c_p}{k}$ is the Prandtl number and $Le = \frac{\vartheta}{D_B}$ is the Lewis number.

The wall shearing stress (stretching sheet) is given by

$$f_{\eta} = 1 + Lf_{\eta\eta}$$

$$\tau_w = (\vartheta u_y)_{y=0}$$

The local skin-friction coefficient is written as

$$C_f = \frac{\tau_w}{\rho u_w^2} = \mathrm{Re}_x^{-1/2} \left(1 + \frac{1}{\beta}\right) f_{\eta\eta}(0). \tag{11}$$

The local heat flux is given by

$$q_w = -k(T_y)_{y=0} = -k\sqrt{\frac{a}{\vartheta}}(T_w - T_\infty)\theta_{\eta}(0)$$

The local Nusselt number is written as

$$Nu_x = \frac{q_w x}{k(T_w - T_\infty)} = -\mathrm{Re}_x^{-1/2}\theta_{\eta}(0) \tag{12}$$

The mass flux is given by

$$q_w = -D_B(C_y)_{y=0} = -D_B\sqrt{\frac{a}{\vartheta}}(C_w - C_\infty)\phi_\eta(0)$$

The Sherwood number is written as

$$Sh_x = \frac{xq_m}{D_B(C_w - C_\infty)} = -\mathrm{Re}_x^{-1/2}\phi_\eta(0) \qquad (13)$$

Here $\mathrm{Re}_x = \dfrac{xu_w}{\vartheta}$ is the Reynolds number.

3. Numerical Analysis

In this study addresses the set of Non-dimensional Non-linear couple boundary layer equations with boundary conditions does not possess a closed form analytical solution. The governing partial differential equations can be converted to closed form equations by using Similarity transformations then it has been solved numerically by Runge-Kutta sixth order integration technique. The entire numerical analysis is done by using Mathematica computer language. From the process of numerical computation the fluid velocity, the temperature, the concentration, the Skin friction coefficient, the Nusselt number and Sherwood number are proportional to $f''(\eta), \theta(\eta), \phi(\eta)$.

4. Results and discussion

In order to provide a clear insight of the present problem. The dimensionless velocity, temperature, concentration, skin friction, Nusselt number, Sherwood number are analyzed through graphically. The various values of Angle parameter(γ), Casson parameter (â) and Slip parameter (L)are shown in graphical figures.

The effects of Angle parameter (γ) on the dimensionless velocity, temperature, concentration profiles are presented in fig.4.1, fig.4.2, and fig.4.3. In this figure illustrates the increasing values of angle parameter decrease the velocity profile and increase the temperature and concentration profiles. The effects of angle parameter on the dimensionless Skin friction coefficient, Nusselt and Sherwood numbers are presented in fig.4.4, fig.4.5, and fig.4.6. In this figure illustrates the increasing values of angle parameter decrease the Skin friction coefficient, Nusselt number and increase the Sherwood number.
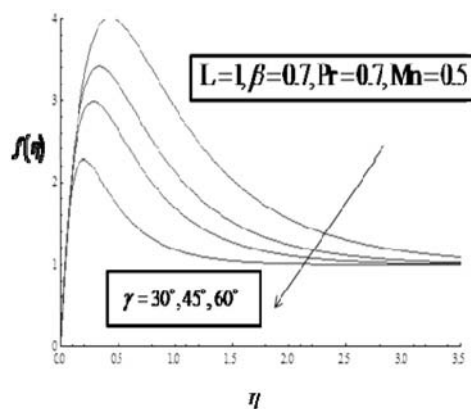
Effects of Angle parameter(γ):

Fig.4.1. Effect of angle parameter (γ) on velocity profile
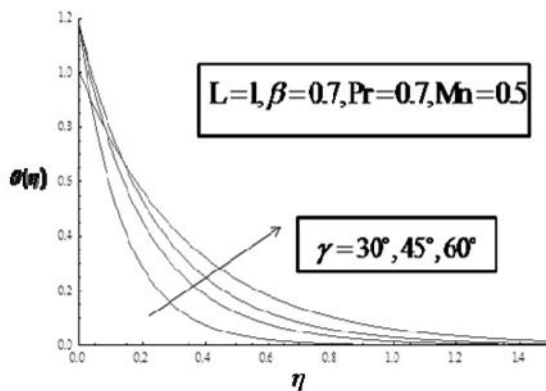

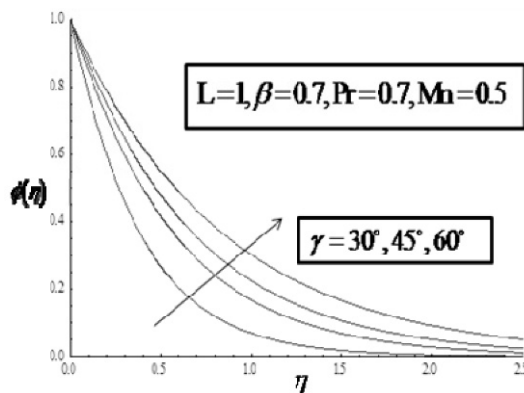Fig.4.2. Effect of angle parameter (γ) on temperature profile

Fig.4.3. Effect of angle parameter(γ) on concentration profile

The effects of Casson parameter (â) on the dimensionless velocity, temperature, concentration profiles are presented in fig.4.7, fig.4.8, and fig.4.9. In this figure illustrates the increasing values of Casson parameter(â) decrease the velocity profile and increase the temperature and concentration profiles.
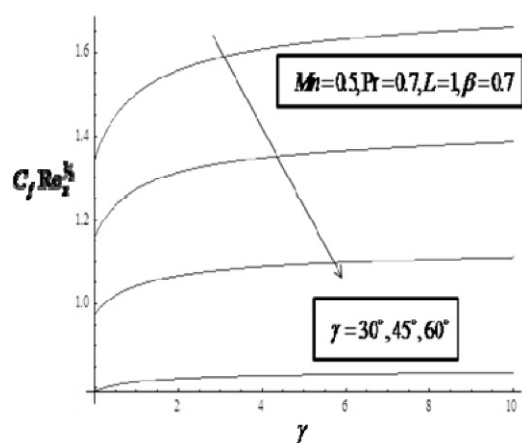
Fig.4.4. Effect of angle parameter (γ) on Skin friction $C_f \, Re_x^{\frac{1}{2}}$

$Mn=0.5, Pr=0.7, L=1, \beta=0.7$

$\gamma=30°, 45°, 60°$

Fig.4.5. Effect of angle parameter (γ) on Nusselt number $Nu_x \, Re_x^{-\frac{1}{4}}$

$Mn=0.5, Pr=0.7, L=1, \beta=0.7$

$\gamma=30°, 45°, 60°$
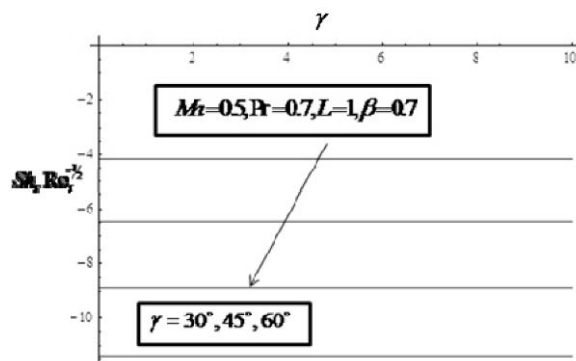
Fig.4.6. Effect of angle parameter (γ) on Sherwood number $Sh_x \, Re_x^{-\frac{1}{2}}$

$Mn=0.5, Pr=0.7, L=1, \beta=0.7$

$\gamma=30°, 45°, 60°$

The effects of Slip parameter(L)on the dimensionless Skin friction coefficient, Nusselt and Sherwood numbers are presented in fig.4.10, fig.4.11, and fig.4.12. In this figure illustrates the increasing values of Slip parameter (L)decrease the Nusselt number and increase the Skin friction coefficient, Sherwood number.

Effects of Casson parameter(â):
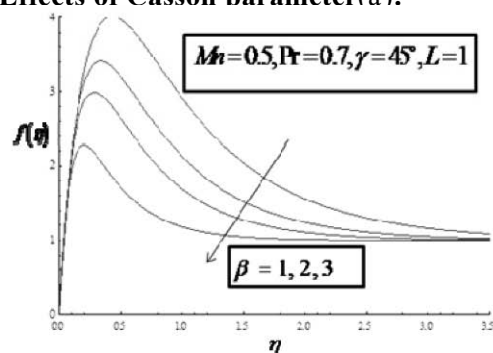
Fig.4.7. Effect of Casson parameter (β) on velocity profile
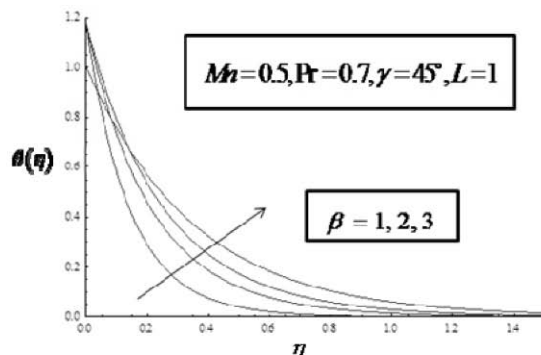
Fig.4.8. Effect of Casson parameter (β) on temperature profile
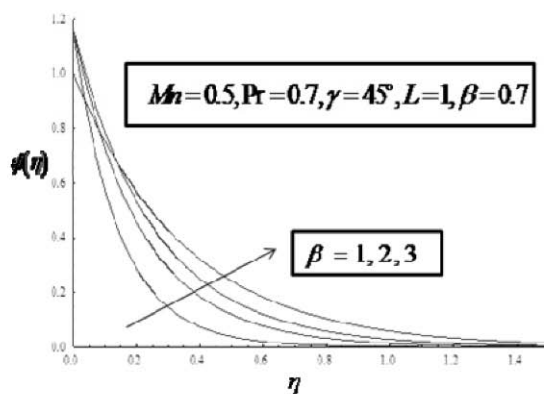
Fig.4.9. Effect of Casson parameter (β) on concentration profile
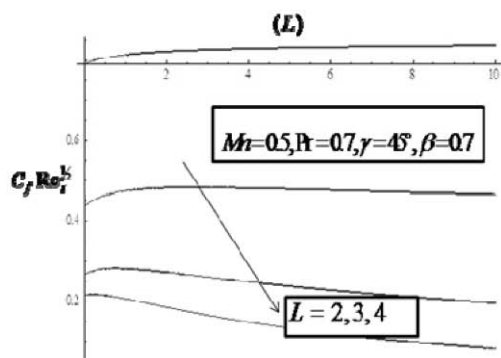

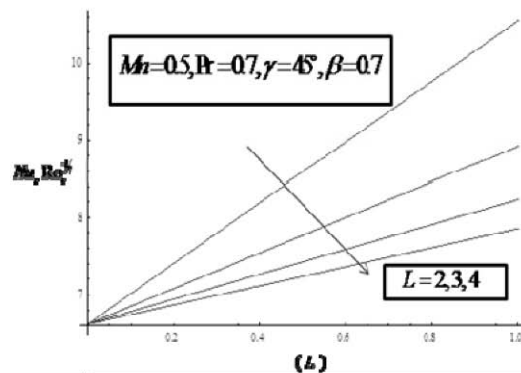Fig.4.10. Effect of Slip parameter (L) on Skin friction $C_f Re_x^{1/2}$

Fig.4.11. Effect of Slip parameter (L) on Nusselt number $Nu_x Re_x^{-1/2}$
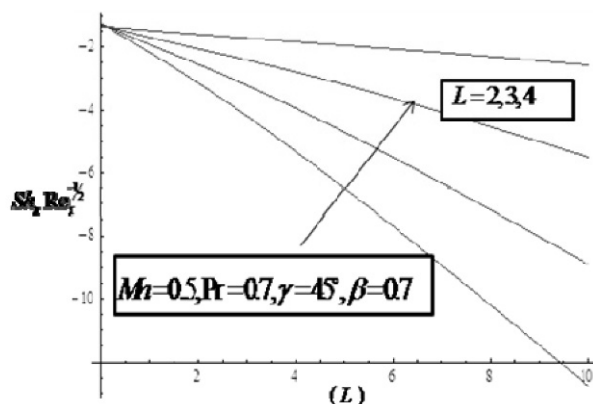
Effects of Slip parameter(L):

Fig.4.12. Effect of Slip parameter (L)
on Sherwood number $Sh_x Re_x^{-\frac{1}{2}}$

4. Conclusion

In this present paper, Slip effects of mass transfer on Casson fluid over a stretching sheet are investigated. Specific results have been obtained using Similarity transformations for different values of pertinent parameters as defined in the transformed governing momentum, energy and concentration equations. The following results can be obtained.

➤ The velocity profile decreases with increasing values of Angle parameter(γ) and Casson parameter(β).

➤ The temperature and concentration profiles enhances with increasing values of Angle parameter (γ) and Casson parameter(β).

➤ The Skin-friction coefficient decreases with increasing values of Angle parameter (γ) and increases with increasing values of Slip parameter(L).

➤ The Nusselt number decreases with increasing values of Angle parameter (γ) and Slip parameter(L).

➤ The Sherwood number increases with increasing values of Angle parameter (γ) and Slip parameter(L).

References

1. **Abdul Hakeem, A.K., Vishnu Ganesh, N., Ganga , B.,** 2015, "Magnetic field effect on second order slip flow of nanofluid over a stretching /shrinking sheet with thermal radiation effect, " J.Magn.Magn.Mater., 381, pp. 243-257.

2. **Bala Anki Reddy, P.,** 2016, "MHD flow of a Casson fluid over an exponentially inclined permeable stretching surface with thermal radiation and chemical reaction," Ain Shams Eng.J., 7(2), pp. 593-602.

3. **Hayat , T., Shehzad , S.H ., Alsaed ,A .,** 2012, " Soret and dufour effects on MHD flow of Casson fluid," Appl. Math. Mech. Eng., 33(10), pp.1301-1312.

4. **Imran ., Bhattacharyya ., Shafie ., Khan .,** 2016, " Unsteady MHD mixed convection slip flow of Casson fluid over a non-linearly stretching sheet embedded in a porous medium with chemical reaction, thermal radiation, heat generation/ absorption and convective boundary conditions," 11(10), PLoS ONE: e0165348.

5. **Pramanik , S .,** 2013, " Casson fluid flow and heat transfer past an exponentially porous stretching surface in presence of thermal radiation," Ain Shams Eng.J., 5(1), pp.205-212.

6. **Sharada ., Bandari .,** 2015 ," MHD mixed convection flow of a Casson fluid over an exponentially stretching surface with the effects of soret, dufour, thermal radiation and chemical reaction," World.J.Mech ., 5, pp.165-177.

7. **Saidulu , N ., Lakshmi , A .,** 2016 ," Slip effects on MHD flow of Casson fluid over an exponentially stretching sheet in presence of thermal radiation, heat source/sink and chemical reaction ," Euro. J. Adv. Engg. Tech ., 3(1), pp.47-55.

8. **Sathesis Kumar, P., Gangadhar , K.,** 2015 ," Effect of chemical reaction on slip flow of MHD Casson fluid over a stretching sheet with heat and mass transfer ," Adv. Appl. Sci. Res ., 6(8), pp.205-223.

9. **Shehzad, S. A ., Hayat , T., Quasim .,** 2013 ," effects of mass transfer on MHD flow of Casson fluid with chemical reaction and suction," Braz.Low.Che.Engg ., 30(1), pp.187-195.

10. **Vijayalaxmi, T., Shankar, B.,** 2016," Effect of aligned magnetic field on slip flow of Casson nanofluid over a nonlinear stretching sheet with chemical reaction," J. Nano., 5(5), pp.696-706.

PROGRAMMABLE DUFFING OSCILLATOR USING FPAA

Sithikraja.R

Abstract

This paper presents the Duffing oscillator implementation in commercially available programmable analog integrated circuit, called field programmable analog array (FPAA). These FPAAs contains an array of similar undedicated analog blocks, and thus it is possible to program both the functionality of each block and interconnects associated with them. It can provide a wide range of analog circuit implementation including chaotic oscillators.

Keywords

Analog blocks-interconnect-chaotic oscillators.

1. Introduction

Since, many Science and Engineering phenomena are dynamic in nature and the study of such a nonlinear system is highly important. In this work the Duffing oscillator is implemented with the help of single analog integrated circuit called Andigm AE221E04. Further, this implementation will increase the usage of Duffing oscillator in an effective way. Last three decade analyzing and synthesizing different phenomena of the dynamical systems yields numerous applications. In communication, chaotic signal are used to make secure communications in both analog and digital communication, image encryptions and cryptography etc. Power electronics also it provides the control over cyclic converters. Finally, since the chaotic system is used to study various dynamical behavior of the system has potential application in cardiology, heart rhythm, EEG analysis, prediction and control of irregular heart activity (chaos-aware defibrillator).

1.1 Duffing Oscillator

The Duffing oscillator is mathematically written as:

Assistant Professor, PG Department of Physics, T.K.S College of Arts and Science, Theni – 625 534, siddiquemscme@gmail.com.

$$\ddot{x} + \delta\dot{x} + \alpha x + \beta x^3 = \gamma \, \cos \omega t \qquad\qquad (1)$$

Where $\ddot{x} = \dfrac{d^2x}{dt^2}$, $x = \dfrac{dx}{dt}$, and δ is a damping ratio, $\gamma \, \cos \omega t$ is a periodic driving force, $\alpha \, \& \, \beta$ are external controlling parameter used to restring nonlinearity of the system.

Furthermore, the Duffing oscillator is a periodically forced oscillator and thus non-autonomous in nature. It exhibits various oscillations starting from small periodic motion to complex chaotic motions when we gradually varying the amplitude of the periodical driven force from low to high [1].

1.2 The FPAA Chip

The chip design technology have led to a novel class of field programmable analog arrays (FPAAs) recently, these FPAAs are accurately programmable analog device that are capable of implementing full scale analog signal processing functions or systems, such as complex chaotic systems [2]. In a quick time, a single FPAA device can be configured to implement several different circuit topologies with the help of desired software. Furthermore, modern FPAAs can also contain analog to digital converters that helps the interfacing of analog systems with the digital world.
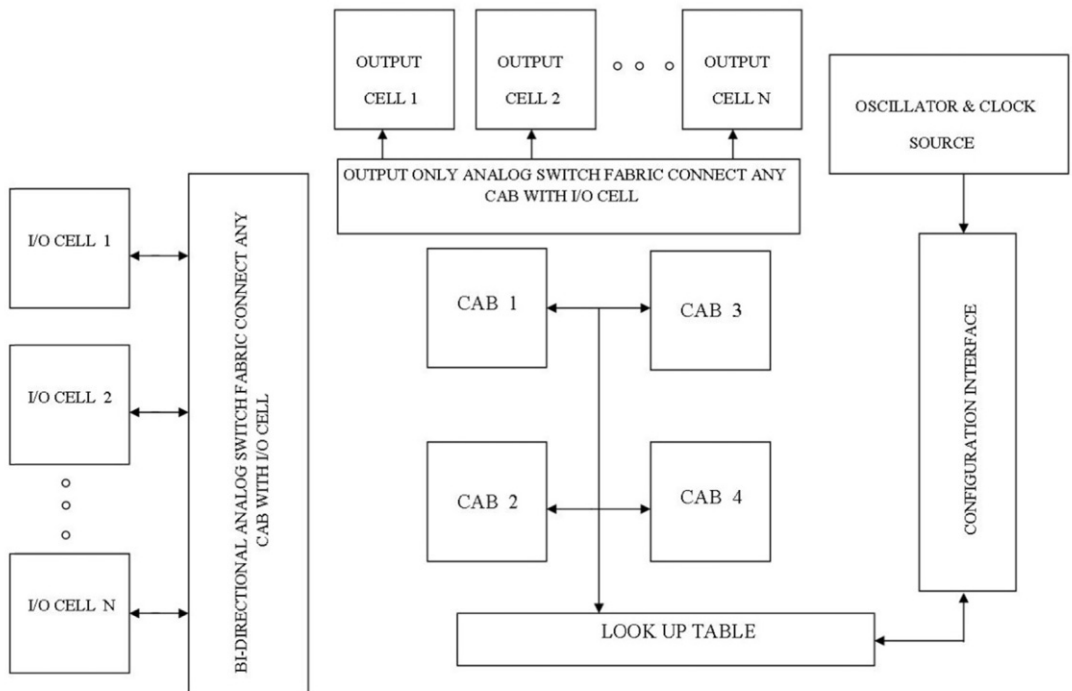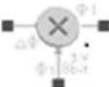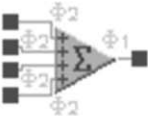

Figure 1. The Andigm AE221E04 chip internal structure

Table 1. The utilized CAB in this work and their transfer functions

Sl. No.	The CAB	Transfer function
1.	Integrator	$\dfrac{\Delta V_{out}}{\Delta t} = \pm K V_{in}$
2.	Multiplier	$V_{out} = M \times V_x \times V_y$
3.	Summing Amplifier	$V_{out} = \pm G_1 V_{in1} \pm G_2 V_{in2} \pm G_3 V_{in3} \pm G_4 V_{in4}$
4.	Inverting Amplifier	$\dfrac{V_{out}}{V_{in}} = -G$

In the digital domain, field programmable gate arrays (FPGAs) are widely used for rapidly prototyping digital hardware as well as in production of digital systems. While Field programmable analog array (FPAA) is providing analog and mixed signal processing based on the switched capacitor technology. Although these analog devices include a small number of configurable analog

blocks (CAB), with few configurable modules CAMs per CAB, they are ideal for rapid and reprogrammable analog design.

Basically, FPAA performs two functions: routing and computation. The routing elements are typically networks of switches connected together by signal lines with the network architecture. Then a large number of computational elements on a single IC, and performance specifications well in excess of that needed in most cases [2, 3]. The transfer function of each CAB utilized in this work explained in the table 1.

The AE221E04 FPAA chip internal structure and connections are shown in Fig. 1. This paper presents a single chip implementation of important basic chaotic system the Duffing oscillator and opens up the root for the programmable analysis and synthesis of complex chaotic system and networks.
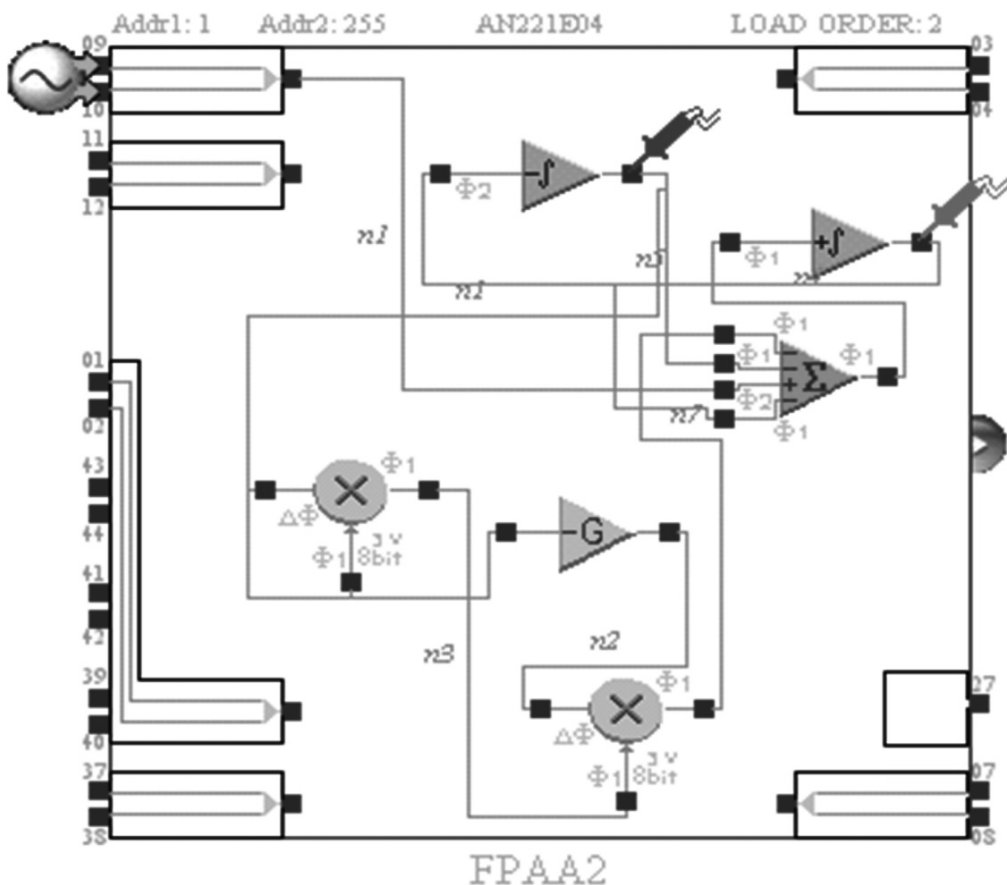
2. FPAA Implementation

Figure 2. The FPAA modeling of Duffing oscillator

The FPAA modeling of Duffing oscillator mathematically explained in equation (1), which is implemented by simple CABs like Integrator, Multiplier, Summing amplifier and Inverting Amplifier as shown in fig. 2. Anadigm Designer 2 software tool is employed here for making the design. Moreover, many other EDA tools are popular in Analog IC design for instance Verilog A etc.
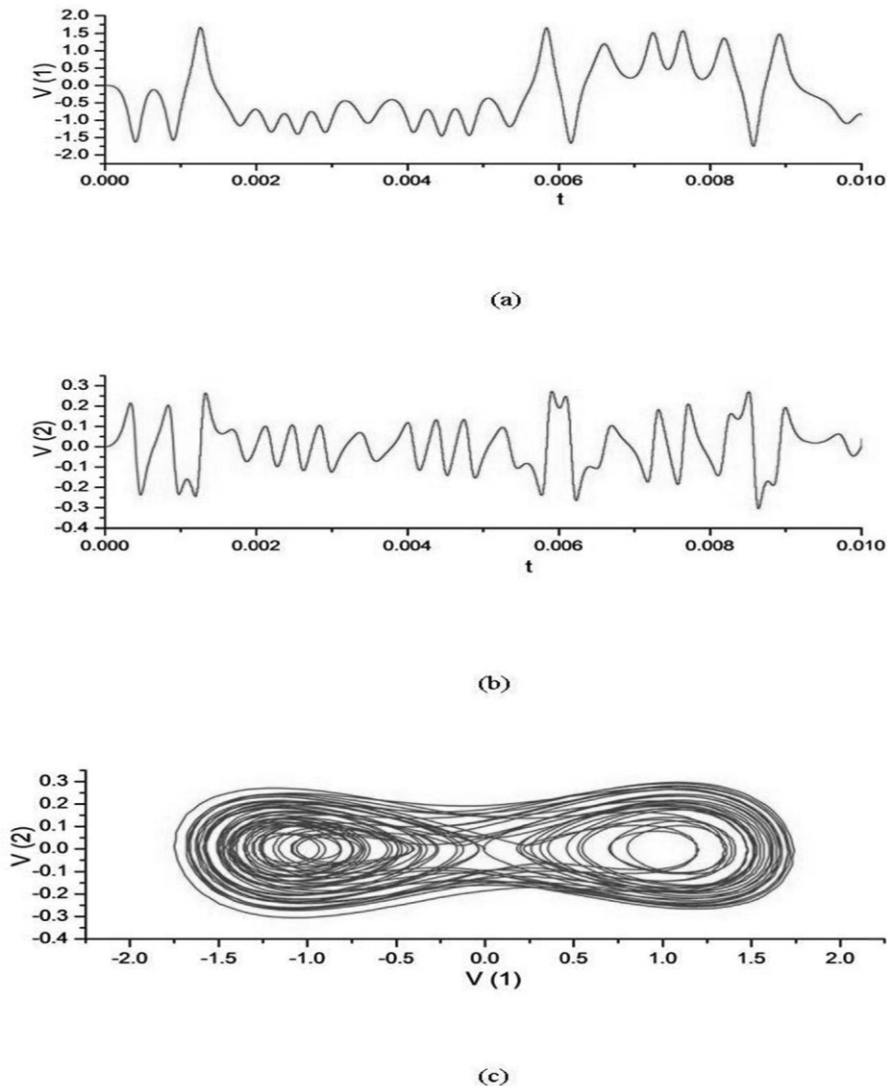
3. Result and Discussion

(a)

(b)

(c)

Figure 3. The simulation result of duffing oscillator. a) time series response for V_1 b) time series response for V_2 and c) double band attractor.

The Duffing oscillator system expressed in the equation (1) has been implemented in FPAA chip via Anadigm Designer2 software. Finally, simulated outputs are obtained as shown in Fig. 3 (a-c). This systems dynamics are depends the damping ratio, the periodic driving force, are the external controlling parameters, whose values are readily adjusted with the help of Anadigm Designer2 software. Finally, simulated outputs of one time series response of V_1 and V_2 and phase prostrate (V_1 vs V_2) are obtained as shown in Fig. 3 (a-c).

4. Conclusion

This paper presents a single chip implementation of important basic chaotic oscillator and opens up the root for the programmable synthesis of complex chaotic system and networks. In this work, simulation result only taken up, One can also implement real time chip implementations as well, where all the input and output are electronically applied such AFO and CRO etc. Since, FPAA device having many CLB quite easily complex chaotic systems and network will be implemented.

References

1. J. A. Goitwald, L. N. Virgin and E. H. Dowell, (1992). Experimental mimicry of Duffing's equation. Journal of Sound and Vibration 158(3), 441-461.

2. Kilic R, (2010). A Practical Guide for Studying Chua's Circuits, World Scientific Publishing Co. Pte. Ltd, Singapore, 55-69.

3. D. Anderson, C. Marcjan, D. Bersch. H. Anderson, P. Hu, Palusinski, D. Gettman, I. Macbeth A. Bratt, (1997). A Field Programmable Analog Array and its Application. Custom Integrated Circuit Conference, 555-558.

4. Recai Kilic, Fatma Yildirim Dalkiran, (2010). Programmable design and implementation of a chaotic system utilizing multiple nonlinear functions. Turk J Elec Eng & Comp Sci, 18(4), 647-655.

5. Anadigm: www.anadigm.com.

OSCILLATION OF THIRD ORDER NONLINEAR DIFFERENTIAL EQUATIONS WITH "MAXIMA"

G.Ayyappan

Abstract

This paper study the oscillatory behavior of third order delay differential equation with "maxima" of the form

$$\left(a(t)(x''(t))^{\gamma}\right) + q(t)\max_{[\tau(t),t]} x(s) = 0, \ t \geq t_0,$$

where γ is ratio of odd positive integers. Examples are included to illustrate the main results.

2010 Mathematics Subject Classification : 34C10, 34K11
Keywords and Phrases: Third order, delay differential equation, oscillation.

1 Introduction

In this paper, we are concerned with the oscillatory behavior of solutions of third order delay differential equation with maxima of the form

$$\left(a(t)(x''(t))^{\gamma}\right) + q(t)\max_{[\tau(t),t]} x(s) = 0, \ t \geq t_0, \qquad (1.1)$$

subject to the following conditions:

(C_1) $a(t), q(t) \in C([t_0,\infty))$, $a(t), q(t)$ are positive, $\tau(t) \in C([t_0,\infty))$, $\tau(t) \leq t$, and $\lim_{t\to\infty} \tau(t) = \infty$ and $\int_{t_0}^{\infty} \dfrac{1}{a^{1/\gamma}(t)}\, dt = \infty$;

(C_2) γ is a quotient of odd positive integers.

By a solution of equation (1.1), we mean a function $x(t) \in C^2[T_x,\infty), T_x \geq t_0$ which has the property $a(t)(x''(t))^{\gamma} \in C^1[T_x,\infty)$ and satisfies equation (1.1) on the interval $[T_x,\infty)$. We consider only those solutions x of equation (1.1) which satisfy condition $\sup\{|x(t)| : t \geq T\} > 0$ for all $T \geq T_x$. We assume that equation (1.1) possesses such a solution. A solution of equation (1.1) is called oscillatory if it has infinitely many zeros on $[T_x,\infty)$; otherwise it is said to be nonoscillatory.

Assistant Professor and Head, Department of Mathematics, Periyar University College of Arts and Science Pappireddipatti- 638 905, Dharmapuri Dt. Tamil Nadu, India. E-mail address: ayyapmath@gmail.com

Differential equations with maximum arise naturally when modelling practical and phenomena problems, in particular, in those which appear in the study of systems with automatic regulation, and automatic control of various technical systems, see [1, 4, 8]. The qualitative theory of these equations is relatively little developed compared to functional differential equations without maxima. The oscillatory behavior of functional differential equations with maxima are studied in [2, 4, 5, 9]. Following this trend, in this paper we obtain sufficient conditions for the oscillatory behavior of solutions of equation (1.1). The results established in this paper extend that of in [3] for equation without maxima.

We say that a nontrivial solution $x(t)$ of (1.1) is strongly decreasing if it satisfies
$$x(t)x'(t) < 0 \qquad\qquad (1.2)$$
for all sufficiently large t and it said to be strongly increasing if
$$x(t)x'(t) > 0. \qquad\qquad (1.3)$$

In Section 2, we obtain some sufficient conditions for oscillation and asymptotic behavior of solutions of third order delay differential equation (1.1). Examples are provided to illustrate the main results in Section 3.

2 Oscillation Results

In this section, we first study the oscillatory behavior of equation (1.1). Without loss of generality we can deal only with the positive solutions of equation (1.1), since the proof for the negative case is similar.

Lemma 2.1 *Let $x(t)$ be a positive solution of equation (1.1). Then $x''(t) > 0$ eventually, and $x(t)$ is either strongly increasing or strongly decreasing.*

Proof. Let $x(t)$ be a nonoscillatory solution of equation (1.1). We may assume that $x(t) > 0$, eventually. Then $\left(a(t)(x''(t))^{\gamma}\right)' < 0$, eventually. Thus $a(t)(x''(t))^{\gamma}$ is decreasing and of one sign and it follows from hypothesis (C_1) and such that such that
$$a(t)(x''(t))^{\gamma} \leq -M, t \geq t_1.$$
Integrating the last inequality from t_1 to t, we obtain
$$x'(t) \leq x'(t_1) - M^{1/\gamma} \int_{t_1}^{t} \frac{1}{a^{1/\gamma}(s)} ds.$$
Letting $t \to \infty$ in the above inequality and using condition (C_1), we see that $x'(t) \to -\infty$. Thus $x'(t) < 0$, which together with $x''(t) < 0$ implies $x(t) < 0$. This contradiction shows that $x''(t) > 0$. Therefore $x'(t)$ is increasing and thus either (1.2) or (1.3) holds, eventually. This completes the proof.

Lemma 2.2 *Assume that* $x(t)$ *is a positive decreasing solution of equation (1.1). If*

$$\int_{t_0}^{\infty}\int_{v}^{\infty}\frac{1}{a^{1/\gamma}(u)}\left(\int_{u}^{\infty}q(s)ds\right)^{1/\gamma}dudv = \infty, \qquad (2.1)$$

then $x(t)$ *tends to zero as* $t \to \infty$.

Proof. It is clear that there exists a finite $\lim_{t\to\infty} x(t) = \ell$. We shall prove that $\ell = 0$. Assume that $\ell > 0$. Integrating equation (1.1) from t to ∞ and using $x(\tau(t)) > \ell$ we obtain

$$a(t)(x''(t))^{\gamma} \geq \int_{t}^{\infty}q(s)\max_{[\tau(s),s]} x(u)ds \geq \ell\int_{t}^{\infty}q(s)ds,$$

which implies

$$x''(t) \geq \frac{\ell}{a^{1/\gamma}(t)}\left(\int_{t}^{\infty}q(s)ds\right)^{1/\gamma}.$$

Integrating the last inequality from t to ∞, we get

$$-x'(t) \geq \ell\int_{t}^{\infty}\frac{1}{a^{1/\gamma}(u)}\left(\int_{u}^{\infty}q(s)ds\right)^{1/\gamma}du.$$

Now integrating from t_1 to t, we arrive at

$$x(t) \geq \ell\int_{t_1}^{t}\int_{v}^{\infty}\frac{1}{a^{1/\gamma}(u)}\left(\int_{u}^{\infty}q(s)ds\right)^{1/\gamma}dudv.$$

Letting $t \to \infty$ we have a contradiction with (2.1) and so we have verified that $\lim_{t\to\infty} x(t) = 0$.

Lemma 2.3 *The function* $x(t)$ *is a negative solution of equation (1.1) if and only if* $-x(t)$ *is a positive solution of the equation*

$$\left(a(t)(x''(t))^{\gamma}\right) + q(t)\max_{[\tau(t),t]} x(s) = 0, \ t \geq t_0.$$

Proof. The proof is obvious.

Theorem 2.1 *If the first order delay differential equation*

$$y'(t) + q(t)\left(\int_{t_0}^{\tau(t)}\frac{\tau(t)-s}{a^{1/\gamma}(s)}ds\right)y^{1/\gamma}(\tau(t)) = 0 \qquad (2.2)$$

is oscillatory, then every solution of equation (1.1) is either oscillatory or strongly decreasing.

Proof. Let $x(t)$ be a nonoscillatory solution of equation (1.1), we may assume that $x(t) > 0$ for all $t \geq t_0$. From Lemma 2.1 we see that $x''(t) > 0$ and $x(t)$ is either strongly increasing or strongly decreasing.
Assume that $x(t)$ is strongly increasing, that is $x'(t) > 0$ eventually. Using the fact that $a(t)(x''(t))^{\gamma}$ is decreasing, we are led to

$$x'(t) \geq \int_{t_1}^{t} x''(s)ds = \int_{t_1}^{t} a^{-1/\gamma}(s)\left(a(s)(x''(s))^\gamma\right)^{1/\gamma} ds$$

$$\geq \left(a(t)(x''(t))^\gamma\right)^{1/\gamma} \int_{t_1}^{t} \frac{1}{a^{1/\gamma}(s)} ds. \qquad (2.3)$$

Integrating (2.3) from t_1 to t, we have

$$x(t) \geq \int_{t_1}^{t} \left(a(s)(x''(s))^\gamma\right)^{1/\gamma} \int_{t_1}^{s} \frac{1}{a^{1/\gamma}(u)} du\, ds$$

$$\geq \left(a(t)(x''(t))^\gamma\right)^{1/\gamma} \int_{t_1}^{t} \frac{(t-s)}{a^{1/\gamma}(s)} ds.$$

There exists a $t_2 \geq t_1$ such that for all $t \geq t_2$, one gets

$$x(\tau(t)) \geq y^{1/\gamma}(\tau(t)) \int_{t_2}^{\tau(t)} \frac{(\tau(t)-s)}{a^{1/\gamma}(s)} ds, \qquad (2.4)$$

where $y(t) = a(t)(x''(t))^\gamma$. Combining (2.4) together with equation (1.1), we see that

$$-y'(t) = q(t) \max_{[\tau(t),t]} x(s)$$

$$= q(t)x(t) \geq q(t)x(\tau(t))$$

$$\geq q(t)y^{1/\gamma}(\tau(t)) \int_{t_2}^{\tau(t)} \frac{(\tau(t)-s)}{a^{1/\gamma}(s)} ds.$$

Thus the function $y(t)$ is a positive and decreasing solution of the differential inequality

$$y'(t) + q(t)\left(\int_{t_2}^{\tau(t)} \frac{(\tau(t)-s)}{a^{1/\gamma}(s)} ds\right) y^{1/\gamma}(\tau(t)) \leq 0.$$

Hence by Theorem 1 in [7], we conclude that the corresponding differential equation (2.2) also has a positive solution, which contradicts the oscillation of (1.1). Therefore $x(t)$ is strongly decreasing. This completes the proof of the theorem.

Combining Theorem 2.1 and Lemma 2.2 we get the following theorem.

Theorem 2.2 *Assume that (2.1) hold. If equation (2.2) is oscillatory then every solution of equation (1.1) is oscillatory or tends to zero as $t \to \infty$.*

Remark 2.1 *In Theorems 2.1 and 2.2 we have established new comparison principles that enable us to deduce properties of the third order nonlinear differential equation (1.1) from oscillation of the first order nonlinear delay equation (2.2). Consequently taking account of the oscillation criteria for (2.2) we get immediately results for the properties of (1.1) investigated.*

Theorem 2.3 *Let $\tau'(t) > 0$. Assume that there exists a function $\xi(t) \in C^1([t_0,\infty))$ such that*

$$\xi'(t) \geq 0,\ \xi(t) > t,\ and\ \eta(t) = \tau(\xi(\xi(t))) < t. \qquad (2.5)$$

If both the first order delay equation (2.2) and

$$z'(t) + \left(\int_t^{\xi(t)} \frac{1}{a^{1/\gamma}(s)} \left(\int_s^{\xi(s)} q(u)du \right)^{1/\gamma} ds \right) z^{1/\gamma}(\eta(t)) = 0 \qquad (2.6)$$

are oscillatory, then every solution of equation (1.1) is oscillatory.

Proof. Let $x(t)$ be a nonoscillatory solution of equation (1.1) and we may assume that $x(t) > 0$. From Theorem 2.1, we see that $x(t)$ is strongly decreasing (that is $x'(t) < 0$). Integration of (1.1) from t to $\xi(t)$ yields

$$a(t)(x''(t))^\gamma \geq \int_t^{\xi(t)} q(s) \max_{[\tau(s),s]} x(u)ds \geq x(\tau(\xi(t))) \int_t^{\xi(t)} q(s)ds.$$

Then

$$x''(t) \geq \frac{x^{1/\gamma}(\tau(\xi(t)))}{a^{1/\gamma}(t)} \left(\int_t^{\xi(t)} q(s)ds \right)^{1/\gamma}.$$

Integrating from t to $\xi(t)$ once more, we get

$$-x'(t) \geq \int_t^{\xi(t)} \frac{x^{1/\gamma}(\tau(\xi(s)))}{a^{1/\gamma}(s)} \left(\int_s^{\xi(s)} q(u)du \right)^{1/\gamma} ds$$

$$\geq x^{1/\gamma}(\tau(\xi(\xi(s)))) \int_t^{\xi(t)} \frac{1}{a^{1/\gamma}(s)} \left(\int_s^{\xi(s)} q(u)du \right)^{1/\gamma} ds$$

$$\geq x^{1/\gamma}(\eta(t)) \int_t^{\xi(t)} \frac{1}{a^{1/\gamma}(s)} \left(\int_s^{\xi(s)} q(u)du \right)^{1/\gamma} ds.$$

Finally integrating from t to ∞, one obtains

$$x(t) \geq \int_t^\infty x^{1/\gamma}(\eta(s)) \int_s^{\xi(s)} \frac{1}{a^{1/\gamma}(u)} \left(\int_u^{\xi(u)} q(v)dv \right)^{1/\gamma} duds. \qquad (2.7)$$

Let us denote the right hand side of (2.7) by $z(t)$. Then $z(t) > 0$ and one can easily verify that $z(t)$ is solution of the differential inequality

$$z'(t) + \left(\int_t^{\xi(t)} \frac{1}{a^{1/\gamma}(s)} \left(\int_s^{\xi(s)} q(u)du \right)^{1/\gamma} ds \right) z^{1/\gamma}(\eta(t)) \leq 0.$$

Then Theorem 1 in [7] shows that the corresponding differential equation (2.6) also has a positive solution, which is a contradiction. This completes the proof.

Remark 2.2 *When choosing $\xi(t)$ we are very particular about two conditions $\xi(t) > t$ and $\tau(\xi(\xi(t))) < t$ holding. Unfortunately there is no general rule as regards how to choose function $\xi(t)$ to obtain the best results for oscillation of (2.6). We suggest that function $\xi(t)$, should be choose to the inverse function of $\xi(t)$.*

3 Examples
In this section, we present some examples to illustrate the importance of the main results.

Example 3.1 *Consider the third order delay differential equation with maxima*

$$\left(tx''(t)\right)+\frac{2}{t^2}\max_{[t/2,\,t]}x(s)=0,\ t\geq 0,\qquad (3.1)$$

where $a(t)=t, q(t)=\frac{2}{t^2}, \tau(t)=\frac{t}{2}$, and $\gamma=1$. Now, one can easily verify that condition (2.1) satisfied, and equation (2.2) reduces to

$$y'(t)+\frac{1}{t}\left(ln(t/2)-1+\frac{2}{t}\right)y(t/2)=0.\qquad (3.2)$$

By Theorem 2.1.1 of [6], guarantees oscillation of equation (3.2) provided

$$\lim_{t\to\infty}\frac{1}{2}\left(ln(2)ln(t^2/8)+2ln(1/2)\right)>\frac{1}{e},$$

which is clearly satisfied and according to Theorem 2.1 every nonoscillatory solution of equation (3.1) tends to zero as $t\to\infty$.

Example 3.2 *Consider the third order delay differential equation with maxima*

$$(tx''(t))'+\frac{3}{t^2}\max_{[t/4,\,t]}x(s)=0,\ t\geq 1,\qquad (3.3)$$

where $a(t)=t, q(t)=\frac{3}{t^2}, \tau(t)=\frac{t}{4}$, and $\gamma=1$. Choosing $\xi(t)=\frac{3}{2}t,$ equation (2.6) now reduces to

$$z'(t)+\frac{1}{3t}z\left(\frac{9}{16}t\right)=0,$$

and the condition

$$\frac{2}{3}ln\left(\frac{4}{3}\right)>\frac{1}{e}\qquad (3.4)$$

guarantees its oscillation by Theorem 2.3 if (3.4) holds.

Acknowledgement

References

1. Arolska.M., and Bainov.D.,(1980) Periodic solutions of differential equations with "maxima", *Plovdiv. Univ. Nauchn Trud.,* **18**, 143-153.

2. Arul.R., and Mani.M., (2014) On the oscillatio of third order quasilinear delay differential equations with "maxima", *Malaya J. Mathematik,* **2**, 489-496.

3. Baculikova.B., and Dzurina.J., (2011) Oscillation of third order nonlinear differential equations, *Appl. Math. Lett.,* **24**, 446-470.

4. Bainov.D., and Hristova.S.G., (2011) Differential Equations with "Maxima", *CRC Press, New York*.

5. Bainov.D., and Zahariev.A., (1984) Oscillation and asymptotic properties of a class of functional differential equations with "maxima", *Czech. Math. J.,* **34**, 247-251.

6. Ladde.G.S., Lakshmikantham.V., and Zhang.B.G., (1987) Oscillation Theory for Differential Equations with Deviating Arguments, *Dekker, New York*.

7. Philos.Ch.G., (1981) On the existence of nonoscillatory solutions tending to zero at ∞ for differential equations with positive delay, *Arch. Math.,* **36**, 168-178.

8. Popov.E.P., (1996) Automatic Regulation and Control, *Nauka, Moscow*.

9. Zhang.B., and Zhang.G., (2000) Qualitative properties of functional differential equations with "maxima", *Rocky Mountain J. Math.,* **29**, 357-369.

FORM IV

Statement about ownership and other particulars

1.	Place of publication	Chennai
2.	Periodicity of its publication	biannually
3.	Printer's Name	D.RAMANATHAN
	Nationality	Indian
	Address	Alamu Printing Works,
		9/5, Iyyah Street, Royapettah, Chennai - 600 014
4.	Publisher's Name	Thiru.T.Anbalagan, I.A.S.
	Nationality	Indian
	Address	Tamil Nadu State Council for Higher Education
		Lady Wellington College Campus, Chennai - 600 005
5.	Editor's name	Thiru.T.Anbalagan, I.A.S.
	Nationality	Indian
	Address	Tamil Nadu State Council for Higher Education
		Lady Wellington College Campus, Chennai - 600 005

6. Names and addresses of individuals who own the newspaper and partners or shareholders holding more than one per cent of the total capital.

I, Thiru.T.Anbalagan, hereby declare that the particulars given above are true to the best of my knowledge and belief.

Date........................   Signature of Publisher

SUBSCRIPTION RATES

Inland (Rs.)	One year	Life time
Individuals	₹ 90/-	₹ 1000/-
Institutions	₹ 150/-	₹ 1500/-

Outstation cheques should include ₹ 30/- towards bank commission

Remittance should be payable to Member Secretary, TANSCHE, Chennai

Please mail your subscription order/ enquires to :

The Member - Secretary

Tamil Nadu State Council for Higher Education

Lady Wellington College Campus, Kamarajar Salai, Chennai 600 005

Web site : www.tnuniv.ac.in

Email : tansche_edu@yahoo.co.in

Phone No 2844 5570

Fax No 44 2844 6486